Biogeosciences
Discussions

EGU
Open Access

1   **Reconstructing past variations in environmental conditions and paleoproductivity**

2   **over the last ~8000 years off Central Chile (30° S)**

3

4   Práxedes Muñoz[1,2], Lorena Rebolledo[3,4], Laurent Dezileau[5], Antonio Maldonado[2],

5   Christoph Mayr[6,7], Paola Cárdenas[4,8], Carina B. Lange[4,9,10], Katherine Lalangui[9], Gloria

6   Sanchez[11], Marco Salamanca[9], Karen Araya[1,5], Ignacio Jara[2], Gabriel Vargas[12], Marcel

7   Ramos[1,2].

8

9   [1]Departamento de Biología Marina, Universidad Católica del Norte, Larrondo 1281,

10   Coquimbo, Chile.

11   [2]Centro de Estudios Avanzados en Zonas Áridas (CEAZA), Coquimbo-La Serena,

12   Chile.

13   [3]Departamento Científico, Instituto Antártico Chileno, Punta Arenas, Chile.

14   [4]Centro FONDAP de Investigación Dinámica de Ecosistemas Marinos de Altas

15   Latitudes (IDEAL), Universidad Austral de Chile, Campus Isla Teja, Valdivia, Chile.

16   [5]Laboratoire Géosciences Montpellier (GM), Université de Montpellier, 34095

17   Montpellier Cedex 05, France.

18   [6]Institut für Geographie, FAU Erlangen-Nürnberg, 91058 Erlangen, Germany.

19   [7]Department of Earth and Environmental Sciences & GeoBio-Center, LMU Munich,

20   80333 Munich.

21   [8]Programa Magister en Oceanografía, Universidad de Concepción, casilla 160C,

22   Concepción, Chile.

23   [9]Departamento de Oceanografía, Facultad de Ciencias Naturales y Oceanográficas,

24   Universidad de Concepción, Casilla 160C, Concepción, Chile.

25   [10]Centro de Investigación Oceanográfica COPAS Sur-Austral, Universidad de

26   Concepción, Casilla 160C, Concepción, Chile.

27   [11]Universidad de Magallanes, Punta Arenas, Chile.

28   [12]Departamento de Geología, Universidad de Chile, Santiago, Chile.

29

30   *Correspondence*: Práxedes Muñoz (praxedes@ucn.cl)

31

Abstract

This study aims at establishing past variations of the main oceanographic and climatic features in the Central Chilean coast, using recent sedimentary records of a transitional semi-arid ecosystem susceptible to environmental forcing conditions. Coquimbo (30°S) region is characterized by dry summers and short rainfall periods during winter. The relatively wet-winter climate results from the interactions between the southern westerly winds and the South Pacific Anticyclone (SPA); in summer, the SPA moves southwards while in winter it returns to the north, allowing the passage of storm fronts. This semi-arid zone is strongly affected by variations associated with El Niño-Southern Oscillation (ENSO), caused by seasonal latitudinal changes in the SPA that produce high variability and precipitation in Chilean mid-latitudes. Sediment cores were retrieved in two bays, Guanaqueros and Tongoy, for geochemical analyses including: sensitive redox trace elements, biogenic opal, total organic carbon (TOC), diatoms, stable isotopes of organic carbon and nitrogen. The results suggest a main dry phase of high primary productivity concomitant with high fluxes of organic compounds to the bottom and suboxic-anoxic conditions in the sediments. This period reached a maximum at cal BC ~4500, followed by a continuous increase in wet conditions, low primary productivity and a more oxygenated environment towards the present, being remarkably stronger in the last 2000 years. We suggest that this might be associated with greater El Niño frequencies or similar conditions that increase precipitation, concomitantly with the introduction of oxygenated waters to coastal zones by the propagation of equatorial origin waves.

Keywords: paleoproductivity, paleoredox, trace metals, diatoms, opal, organic carbon, ENSO, Coquimbo, SE-Pacific

1. Introduction

The northern-central Chilean continental margin (18−30°S) has distinct characteristics
in terms of topography, climate and oceanographic conditions, which modulate primary
productivity and the chemical composition of the water column. This zone is
characterized by several foci of high primary production (0.5-9.3 g C m^{-2} d^{-1}; González
et al., 1998; Daneri et al., 2000, Thomas et al., 2001) off Iquique (21°S), Antofagasta
(23°S) and Coquimbo (30°S), resulting from the influx of nutrient-rich waters due to a
semi-permanent upwelling forced by local winds. This productivity takes place close to
the coast above the narrow continental shelf, allowing for the development of relevant
fisheries and accounting for up to 40% of total annual catches in the Chilean margin
(Escribano et al., 2004 and references therein).

Upwelling areas are recognized as special zones where the considerable amount of
organic material produced in the photic zone causes large particle depositions on the
bottom. The remineralization of this organic carbon promotes anoxic/suboxic
environments where chemosynthetic and authigenic reactions occur. The distribution of
chemical compounds present in the sediments and water column are driven by
diagenetic reactions, involving metals and nutrients, related to the destruction of organic
matter and thus are linked to the diagenetic sequence (oxic or anoxic). In the case of
trace metals, these reactions result in soluble or insoluble phases, which are particular
for each metal, depending on the oxidative state of the sediments and bottom waters
(Chester, 1990; Guieu et al., 1998; Wells et al., 1998).

The high productivity observed in these boundary current ecosystems develops and
maintains zones of low dissolved oxygen content known as oxygen minimum zones
(OMZs). These naturally occurring regions are found in the upwelling areas of the
Eastern Boundary Currents, developed along the North and South Pacific Ocean where
their intensity, thickness, and temporal stability vary as a function of latitude (Helly and
Levin, 2004, Ulloa et al., 2012). To the north (e.g. at 21°S) and off Peru, the OMZ is
permanently present, can extend into the euphotic zone and, in the case of northern
Chile and southern Peru, it shows no significant interface with the benthic environment
due to the presence of a narrow continental shelf (Helly and Levin, 2004).

Although ecosystems in Eastern Boundary Currents represent less than 5% of the
ocean's surface, they support regions of unique microbial processes that influence
global element cycles. The nature of the chemical processes that are taking place in
surface sediments and bottom waters establishes the enrichment or depletion of trace

Biogeosciences
Discussions

Open Access

EGU

91   elements within sediments. This could respond to different causes and is not always

92   directly related to the amount of organic carbon that has settled on the bottom.

93   Diagenetic reactions could modify the original extension of metal enrichment that

94   occurs in the upper sediment layer, reflecting the redox conditions during early

95   diagenesis in the sediments (Nameroff et al., 2002) and the environmental conditions of

96   the overlying water, i.e. oxygen content (Zheng et al., 2000; McManus et al., 2002;

97   Siebert et al., 2003), both intimately related to the biological pump.

98   Climatic trends in the last century point to the beginning of a global warming period,

99   mainly observed by a CO_2 increase in the atmosphere (Bolin, 1992; Sarmiento and

100   Gruber, 2002), and corroborated by studies on ice and coral growth records (Mosley-

101   Thompson et al., 2006; Schneider and Steig, 2008; Nurhati et al., 2009). Higher mean

102   temperatures produce the stratification of the oceans suppressing vertical nutrient

103   transport that sustains primary production, as observed after 1999 (Behrenfeld et al.,

104   2006). The El Nino/Southern Oscillation cycles (ENSO) are the most important

105   phenomena with a major impact on sea life – from phytoplankton to marine mammals–

106   and are closely related to changes in atmospheric variables. Their frequency seems to

107   have intensified since cal BP 3200 (Marchant et al., 1999), while extreme variations

108   have been observed in the last 200 yrs. Heavy rainfall episodes normally occur during

109   strong El Niño conditions (Montecinos and Aceituno, 2003), which can also be

110   observed in sedimentary records in northern Chile (23°S; Garreaud and Rutllant, 1996;

111   Vargas et al., 2007). In addition, the deepening of nutrient-rich Equatorial Subsurface

112   Water (ESW) reduces primary productivity in this zone, considered the most productive

113   area in the global ocean promoting biogeochemical changes validated through organic

114   and inorganic sedimentary records (Muñoz et al., 2012 and references therein).

115   Our work focusses on past variations of environmental conditions and marine

116   productivity in recent sedimentary records from a transitional semi-arid ecosystem of

117   Central Chilean coast, susceptible to oceanographic and climatic forcing. The study area

118   (Fig. 1) provides an adequate platform to observe environmental variability within

119   different time scales. We suggest that the low continental inputs allow us to clearly

120   identify wet/dry as well as high/low export primary production periods because

121   sediments in this area receive the organic flux mainly from the upwelling foci in the

122   area. Moreover, the organic flux is restricted to the narrow shelf where low oxygen

123   content has been detected promoting the preservation of inorganic (trace metals) and

124   organic proxies.

2. Study area

125

126 The Coquimbo region constitutes a border area between the most arid zones of northern

127 Chile (Atacama Desert) and the more mesic Mediterranean climate of central Chile

128 (Montecinos et al., 2015). Here, the shelf is narrow and several small bays trace the

129 coast line. Favorable winds throughout the year promote an important upwelling center

130 in the southern part of the region (Lengua de Vaca Point), developing high biomass

131 along a narrow coastal area (Moraga-Opazo et al., 2011), and reaching maximum

132 concentrations of ~20 mg m^{-3} (Torres et al., 2009). High variability in pigment

133 concentrations have been attributed to high variability in physical processes, which

134 modulate Chl-*a* distribution along the coast. The bays of Tongoy and Coquimbo

135 register a bipolar circulation consisting of counter rotating gyres: clockwise to the south

136 of the bays and counterclockwise to the north (Moraga-Opazo et al., 2006; 2011).

137 Additionally, large squirts of photosynthetic pigments are observed from the coast to the

138 open ocean with large eddies acting as retention zones counteracting the transport of

139 Chl-*a* offshore (Rutllant and Montecino, 2002; Marín et al., 2003).

140 The Tongoy and Guanaqueros bays are located at the southern edge of a broad

141 embayment between small islands in the north (29°S; Choros, Damas and Chañaral) and

142 Lengua de Vaca Point in the south (30°S) (Fig. 1), protected from predominant

143 southerly winds. Tongoy Bay is a narrow marine basin (10 km at its maximum width)

144 with a maximum depth of ~100 m. To the northeast lies Guanaqueros Bay, a smaller

145 and shallower basin. Recent oceanographic studies in this zone suggest the relevance of

146 low dissolved oxygen water intrusions from the shelf to shallow waters (Fig. 2), which

147 seem related to sea level decreases resulting from local wind annual cycles at a regional

148 meso-scale (Gallardo et al., 2017)). Furthermore, in the shallow waters of Tongoy Bay,

149 the high primary productivity results in high TOC in the water column that allows for

150 the deposition of fine material on the bottom; TOC increases concurrently with the

151 periods of low oxygen conditions (Fig. 3; Muñoz et al., unpublished data). The spatial

152 and temporal variability of this process is still under study.

153 Sedimentological studies are scarce in the northern-central Chilean shelf. A few

154 technical reports indicate that sediments between 27°S and 30°S are composed of very

155 fine sand and silt with relatively low organic carbon content (<3 and ~5%), except at

156 very limited coastal areas where organic material accounts for around ~16% (Muñoz,

157 unpublished data; FIP2005-61 Report, www.fip.cl). Coastal weathering is the main

158 source of continental input due to scarce river flows and little rainfall in the zone (0.5 to

Biogeosciences

Discussions

Open Access

EGU

159   ~20 mm yr^{-1}; https://es.climate-data.org/location/940/, Fig.1). Freshwater discharges are

160   represented by creeks, which receive the drainage of the coastal range forming wetland

161   areas in the coast and even small estuaries, as observed in Tongoy and Pachingo. These

162   basins cover ~300 and 487 km^2, respectively. The water volume in the estuaries is

163   maintained by the influx of seawater mixed with groundwater supply. No surface flux to

164   the sea is observed. Therefore, freshwater discharge occurs only during high rainfall

165   periods in the coastal zone (DGA, 2011), which normally takes place during El Niño

166   years when higher runoff has been recorded in the area (Valle-Levinson et al., 2000)

167   normally during the June-July-August quarter (Garreaud et al., 2009). In this scenario,

168   marine sediments are often highly influenced by primary production in the water

169   column. This organic input is relevant for the sediment composition and, thus,

170   sedimentary records could clearly reveal the variability in primary production and

171   hence, the oceanographic conditions over the shelf, which ultimately respond to major

172   atmospheric patterns.

173

174   **3. Materials and methods**

175   **3.1. Sampling**

176   Sediment cores were retrieved from two bays in the Coquimbo region: Bahía

177   Guanaqueros (core BGGC5; 30°09' S, 71°26' W; 89 m water depth) and Bahía Tongoy

178   (core BTGC8; 30°14' S, 71°36' W; 85 m water depth) (Fig. 1.), using a gravity corer

179   (KC-Denmark) in May 2015, on board the L/C Stella Maris II owned by the

180   Universidad Católica del Norte. The length of the cores was 126 cm for BGGC5 and 98

181   cm for BTGC8. Both cores were cut along the main axis and a general visual

182   characterization was done. Different textures and color layers were identified using the

183   Munsell color chart.

184   Subsequently, the cores were sliced into 1-cm sections and subsamples were separated

185   for grain size measurements, magnetic susceptibility, trace elements, biogenic opal, C

186   and N stable isotope signatures (δ^{13}C, δ^{15}N), and TOC analyses. The samples were first

187   kept frozen (–20° C) and then freeze-dried before laboratory analyses.

188   The magnetic signal indicates the concentrations and compositions of magnetic

189   minerals and is usually used combined with others detrital proxies -as grain size- to

190   establish changes in sedimentary processes closely controlled by climatic conditions.

191   We considered redox trace elements measurements that respond to local hypoxia (U,

192   Mo and Re) as well as nutrient-type elements, which follow the organic fluxes to the

193   sediments (Ba, Ni Cu, P). Additionally, we measured Fe and Mn relevant in adsorption-

194   desorption and scavenging processes of dissolved elements in the bottom water and

195   sediments. We also measured Ca, K and Pb that have relevant continental sources by

196   coastal erosion, weathering and eolian transport, which is also true for Fe and Mn.

197   Besides, Ca accumulation within the sediments depends on the carbonate productivity

198   and dissolution, being used as paleoproductivity proxy (Paytan, 2008; Govin et al.,

199   2012). We use Al as a normalizing parameter for enrichment/depletion of elements due

200   to its conservative behavior. The crustal contribution and the elements are presented as

201   metal/Al ratios. The authigenic enrichment factor of elements was estimated according

202   to: $EF = (Me/Al)_{sample} / (Me/Al)_{detrital}$; where $(Me/Al)_{sample}$ is the bulk sample metal (Me)

203   concentration normalized to Al content and the denomination "detrital" indicates a

204   lithogenic background (Böhning et al., 2009). Detrital concentrations ($[Me]_{detrital}$ and

205    $[Al]_{detrital}$) were established considering the local TM abundance, which is more accurate

206   than using mean Earth crust values (Van der Weijden, 2002). We used the average of or

207   element concentrations at the surface sediments (0−3 cm) of Pachingo wetland (Table

208   1).

209   Diatoms and siliceous microfossils were identified and counted; jointly with biogenic

210   opal content, they constitute our proxies of siliceous export production. Pollen grains

211   were also identified and counted, and used to identify wet and dry environmental

212   conditions. TOC and stable isotopes of organic matter were used to identify the

213   variability of organic fluxes to the bottom and establish biogeocheemical changes in the

214   organic matter remineralization.

215   [14]C and ^{210}Pb were analyzed at selected sediment levels and foraminifera species were

216   selected for radiocarbon analyses (Table 2).

217

218   **3.2, Geochronology (^{210}Pb and ^{14}C)**

219   [210]Pb activities were quantified through alpha spectrometry of its daughter [210]Po in

220   secular equilibrium with ^{210}Pb, using [209]Po as a yield tracer (Flynn, 1968). The chemical

221   procedure considered a total digestion of the sediment samples and then autoplated onto

222   silver disks at ~75°C for 3 three hours in the presence of ascorbic acid. The [210]Po

223   activity was counted in a CANBERRA QUAD alpha spectrometer, model 7404, until

224   the desired counting statistics was achieved (4−10% 1σ errors) in the Chemical

225   Oceanography Laboratory of Universidad de Concepción. [210]Po activity –assumed to be

226   in secular equilibrium with [210]Pb– was calculated using the ratio between natural

227   radionuclide and the tracer, which is multiplied by the activity of the tracer at the time

228   of plating. The period elapsed between plating and counting produces ^{210}Po decay (half-

229   life: 138 days) and between sampling and plating ^{210}Pb decay (half-life: 22.3 yr);

230   counting was corrected to these elapsed times even when there was a short time period

231   between the collection date and the time of sample analysis (less than one year). Ages

232   were estimated using the inventories of the activities in excess (^{210}Pb$_{xs}$, unsupported),

233   based on the Constant Rate of Supply Model (CRS, Appleby and Oldfield, 1978).

234   Unsupported activities were determined as the difference between ^{210}Pb and ^{226}Ra

235   activities measured in some sediment column intervals. ^{226}Ra was measured with a

236   gamma spectrometry at the Laboratoire Géosciences of the Université de Montpellier

237   (France). Standard deviations (SD) of the ^{210}Pb inventories were estimated propagating

238   counting uncertainties (Bevington and Robinson, 1992) (Table S1, supplementary data).

239   Radiocarbon measurements were performed on a mix of planktonic foraminifera species

240   in core BGGC5 whereas the benthic foraminifera species *Bolivina plicata* was selected

241   for core BTGC8 (Table 2). Freeze-dried sediment was washed over a 63 µm mesh-size

242   sieve and dried after washing at 50°C. At least 2 mg of mixed planktonic foraminifera

243   were picked from the 125−250 µm fraction. The samples were submitted to the National

244   Ocean Sciences AMS Facility (NOSAMS) of the Woods Hole Oceanographic

245   Institution (WHOI). The Fraction Modern (Fm) was corrected by the δ^{13}C value, and

246   ages were calculated using 5568 (yrs) as the half-life of radiocarbon. The ages were

247   converted to calendar years before present using the calibration curve

248   Calpal2007_HULU (Jöris and Weninger, 1998), and considering an age reservoir effect

249   that compares the ^{14}C value in the foraminifera core with ages estimated from the CRS

250   model. The deviation from the global mean reservoir age (DR) was estimated

251   subtracting the value corresponding to the age obtained with the CRS model in the

252   marine 13.14c curve (Reimer et al., 2013) from the apparent ^{14}C age measured at depths

253   of 5 and 10 cm for cores BTGC8 and BGGC5, respectively (Sabatier et al., 2010; Table

254   3). The time scale was obtained according to the best fit of ^{210}Pb$_{xs}$ curves and ^{14}C points,

255   using the CLAM 2.2 software and Marine curve 13C (Reimer et al, 2013), and

256   considering a global reservoir of 441 years (Fig. 4).

257

258   **3.3. Geophysical characterization**

Biogeosciences

Discussions

EGU

Open Access

259   Magnetic susceptibility ($SI \times 10^{-8}$) was measured with a Bartington Susceptibility Meter

260   MS2E in the Sedimentology Laboratory at Centro Eula, Universidad de Concepción.

261   Mean values from three measurements were calculated for each sample.

262   Grain size was determined using a Mastersizer 2000 laser particle analyzer, coupled to a

263   Hydro 2000−G Malvern in the Sedimentology Laboratory of Universidad de Chile.

264   Skewness, sorting and kurtosis were evaluated using the GRADISTAT statistical

265   software (Blott and Pye, 2001), which includes all particle size spectra.

266

3.4. Trace elements analysis

268   Trace element analyses were performed by ICP-MS (Inductively Coupled Plasma-Mass

269   Spectrometry) and carried out at Université de Montpellier 2, France (OSU

270   OREME/AETE regional facilities), using an Agilent 7700x. About 50 mg of samples

271   and geochemical reference materials (UBN, BEN and MAG1) were dissolved twice

272   through the conventional digestion method using a concentrated $HF-HNO_3-HClO_4$ mix

273   (1:1:0.1) in Savillex screw-top Teflon beakers at 120°C, on a hot plate during 48h.

274   Following digestion, the samples were subjected to three evaporation steps in order to

275   remove fluorine. Shortly before analysis, samples were dissolved in 2 ml of

276   concentrated HNO_3 and transferred to 20 ml polypropylene bottles. Final sample

277   preparation was undertaken by dilution with ultrapure water to a sample-solution weight

278   ratio of 1: 4000-5000 and the addition of a known weight of internal standard solution

279   consisting of 1 ppb of In and Bi. Internal standardization used ultra-pure solution

280   enriched in In and Bi, both elements whose natural abundances in geological samples

281   do not contribute significantly to the added internal standard. This is used to deconvolve

282   mass-dependent sensitivity variations of both matrix and instrumental origin, occurring

283   during the course of an analytical session.

284   Sample introduction uses a peristaltic pump, a micro-nebulizer and a cooled double-

285   pass Scott type spray chamber. The uptake time (typically 45 s) is set to facilitate stable

286   analyte signals prior to a 120 seconds analysis for each sample. Elements with an

287   atomic mass lower than 80 were analyzed in collision mode using He; heavier elements

288   were analyzed in no-gas mode. A wash out procedure consisting of 60 seconds with

289   HNO_3 10% and 120 seconds with 2% HNO_3 has been found appropriate to achieve

290   instrument blank level. The total time for analysis of a single sample solution is *c.* 3

291   minutes. Mean concentrations for the analyzed samples were determined by external

292   calibrations prepared daily from multi- and mono-elemental solutions, with

293   concentrations in the range of 0.05−10 ppb for trace elements and of 1−10 ppm for

294   major elements (Ca, K). Polyatomic interferences were controlled by running the

295   machine at an oxide production level <1%. Typical analytical precisions attained by this

296   technique are generally between 1% and 3%, relative standard deviation. Accuracy has

297   been assessed with an analysis of international reference materials and results show

298   agreement generally better than ±5% with reference values.

299

300   **3.5. TOC and stable isotopes**

301   TOC and stable isotope (δ^{15}N and δ^{13}C) analyses were performed at the Institut für

302   Geographie, Friedrich Alexander Universität (FAU) Erlangen-Nürnberg, Germany. Dry

303   material was placed into tin and silver capsules for N and C analyses respectively, and

304   combusted at 1060° C in a continuous helium flow in an elemental analyzer (NC2500,

305   Carlo Erba), in the presence of chromium oxide and silvered cobalt oxide. The resulting

306   gases, were passed over copper wires at 650° C to reduce nitrogen and excess oxygen.

307   Thereafter, water vapor was trapped with $Mg(ClO_4)_2$ and the remaining gases (N_2 and

308   CO_2) were separated in a gas chromatography column at 45° C. N_2 and CO_2 were

309   passed successively via a ConFloII interface into the isotope-ratio-mass spectrometer

310   (Delta Plus, Thermo-Finnigan) and isotopically analyzed. Carbon and nitrogen contents

311   were determined from the peak-area-versus-sample-weight ratio of each individual

312   sample and calibrated with the elemental standards cyclohexanone-2,4-

313   dinitrophenylhydrazone ($C_{12}H_{14}N_4O_4$) and atropine ($C_{17}H_{23}NO_3$) (Thermo Quest). A

314   laboratory-internal organic standard (Peptone) with known isotopic composition was

315   used for final isotopic calibrations. Stable isotope ratios are reported in the δ notation as

316   the deviation relative to international standards (Vienna Pee Dee Belemnite for δ^{13}C and

317   atmospheric N_2 for δ^{15}N), so δ^{13}C or δ^{15}N = [(R sample/R standard) − 1] x 10^3, where R

318   is ^{13}C/^{12}C or ^{15}N/^{14}N, respectively. Typical precision of the analyses was ±0.1‰ for

319   δ^{15}N and δ^{13}C.

320

321   **3.6. Biogenic opal**

322   Biogenic opal was estimated following the procedure described by Mortlock and

323   Froelich (1989) with a slight modification, which consists in extracting 50 mg of

324   sediment with 1 M NaOH (instead of 2 M Na_2CO_3) at 85°C for 5 hours. Extraction and

325   analysis by molybdate-blue spectrophotometry (Hansen and Koroleff, 1999) were

326   conducted at the laboratories of Marine Organic Geochemistry and Paleoceanography,

327   University of Concepción, Chile. Values are expressed as biogenic opal by multiplying

328   the Si (%) by 2.4 (Mortlock and Froelich, 1989). Analytical precision was ± 0.5%.

329   Accumulation rates were determined based on sediment mass accumulation rates and

330   amount of opal at each core section in %.

331

332   **3.7. Diatoms and siliceous microfossils**

333   Smear slides for qualitative abundances of siliceous microfossils were carried out every

334   centimeter following the Ocean Drilling Program (ODP) protocol described by

335   Mazzullo et al. (1988.) To determine the quantitative abundance of siliceous

336   microfossils (diatoms, silicoflagellates, sponge spicules, crysophyts and phytoliths), ~

337   0.5 g of freeze-dried sediment was treated according to Schrader and Gersonde (1978).

338   Samples were chosen every ~4, 8 and 12 cm for BGGC5 and at an average of 6 cm for

339   BTGC8. Permanent slides were prepared by placing a defined sample volume (0.2 ml)

340   onto microscope slides that were then air-dried and mounted with Naphrax mounting

341   medium (refraction index =1.3). Siliceous microfossils were identified and counted

342   under an Olympus CX31 microscope with phase contrast. 1/5 of the slides were counted

343   at 400X for siliceous microfossils and one transect at 1000x was counted for

344   *Chaetoceros* resting spores. Two slides per sample were counted; the estimated

345   counting error was 15%. Total diatom abundances are given in valves g^{-1} of dry

346   sediments.

347

348   **3.8. Pollen**

349   Sample preparation for pollen analysis was conducted following the standard

350   methodology for sediment samples (Faegri and Iversen, 1989), which includes

351   deflocculating with 10% KOH, carbonate dissolution with a 5% HCl treatment, silica

352   dissolution with 30% HF, and cellulose removal *via* acetolysis reactions. Samples were

353   mounted with liquid glycerol and sealed permanently with paraffin wax. Pollen

354   identification was conducted under a stereomicroscope 400 fold magnification with the

355   assistance of the Heusser (1971) pollen catalogue. A total of 100-250 terrestrial pollen

356   grains were counted on each sample depending on their abundance. Pollen percentage

357   for each taxon was calculated from the total sum of terrestrial pollen. The percentage of

358   aquatic pollen and fern spores was calculated based on the total terrestrial sum plus the

359   respective group. Pollen percentage diagrams were generated using the Tilia software

360   (E. Grimm, Illinois State Museum, Springfield, IL. USA). The diagram was divided into

361   "zones" based on the identification of the most important changes in pollen percentage

362   and assisted by a cluster ordination (CONISS) performed by the same software.

363   We further summarize pollen-based precipitation trends by calculating a Pollen

364   Moisture Index (PMI), which is defined as the normalized ratio between Euphorbiaceae

365   (wet coastal scrubland) and Chenopodiaceae (arid scrubland). Thus, positive (negative)

366   values of this index indicate the relative expansion (reduction) of coastal scrubland

367   under relatively wetter (drier) conditions.

368

369   **4. Results**

370   **4.1. Geochronology**

371   $^{210}Pb_{xs}$ (unsupported activity) was obtained from the surface down to 8 cm depth in the

372   two cores, with an age of ~cal AD 1860 at 7 cm in both of them (Table S1). Greater

373   surface activities were obtained for core BGGC5 (13.48 ± 0.41 dpm g^{-1}) compared to

374   core BTGC8 (5.80 ± 0.19 dpm g^{-1}), showing an exponential decay with depth (Fig. 4).

375   A recent sedimentation rate of 0.11±0.01 cm yr^{-1} was estimated.

376   The age reservoir estimation was similar for both cores, 441 and 442 years for BGGC5

377   and BTGC8, respectively (Table 3). The age model provided a maximum age of cal BC

378   6300 for core BGGC5, and cal BC 5760 for core BTGC8 (Fig. 4). A mean

379   sedimentation rate of 0.02 cm yr^{-1} was estimated for core BGGC5, with a period of

380   relative low values (0.01 cm yr^{-1}) between cal BC 4000 and 2000. For BTGC8,

381   sedimentation rates were less variable and around 0.013 cm yr^{-1} in the entire core.

382

383   **4.2. Geophysical characterization**

384   The sediments retrieved from the bays showed fine grains in the range of very fine sand

385   and silt in the southern areas. There, the grain size distribution was mainly unimodal,

386   very leptokurtic, better sorted and skewed to fine grain when compared to sediments

387   from the northern areas. Sediment cores obtained from the northern areas were sandy

388   (coarse sand and gravel), with abundant calcareous debris. Longer cores of soft

389   sediment were retrieved at the southern areas (BGGC5 and BTGC8), where the silty

390   component varied between 40 % and 60 % (Fig. 1 and 5a,b). The clay component was

391   very low at both cores (<2%). The sediment's color ranged from very dark grayish

392   brown to dark olive brown (2.5Y 3/3−3/2) at Guanaqueros Bay (BGGC5) and from dark

393   olive gray to olive gray (5Y 3/2−4/2) at Tongoy Bay (BTGC8). Visible macro-remains

394   (snails and fish vertebrae) were found and weak laminations were identified at both

395   cores. The magnetic susceptibility showed higher values close to the surface, up to 127

396   SI x10^{-8} at BGGC5 and relative lower values (85 SI x10^{-8}) at BTGC8. At greater depths,

397   however, the values were very constant, around 5−8 x10^{-8} SI at BGGC5 core and

398   around 12−20 x10^{-8} SI at BTGC8 core. In both cores, susceptibility increases

399   substantially after cal AD 1800 (Figs. 5a, 5b). Lower bulk densities were estimated at

400   the core BGGC5 (0.7−0.9 g cm^{-3}) compared to the core BTGC8 (>1 g cm^{-3}) (Fig. 5a,

401   5b). In accordance with this, the mean grain size was 60−80 μm at Guanaqueros Bay

402   (BTGC8), compared to 50−60 μm at Tongoy Bay (BGGC5). Both cores were

403   negatively skewed, with values of -1 to -1.2 at BGGC5, and -1 to -2.5 at BTGC8. Minor

404   increases towards coarser grain size were observed in the last 2000 years, especially at

405   Tongoy Bay (BTGC8). In both cases, grain size distributions were strongly leptokurtic.

406   Ca/Fe ratio also diminished in time, except at core BTGC8 where it was only observed

407   during the last ~3000 years. The diminishing of the Ca/Fe ratio is due to a decrease in

408   Ca content mainly but also because of a slight increase in Fe within the sediments (Figs.

409   6a, 6b).

410

411   **4.3. Biogenic components**

412   **4.3.1. Siliceous microfossils and biogenic opal**

413   Total diatom abundance fluctuated between 5.52 x10^5 and 4.48 x10^7 valves g^{-1} in core

414   BGGC5. Total diatom abundance showed a good correlation with biogenic opal content

415   at BGGC5 (R^2 =0.52, P<0.5), with the highest values from 72−74 cm to the bottom of

416   the core, corresponding to cal BC 3390−3790. In contrast, diatom abundance and

417   biogenic opal were much lower in core BTGC8 (< 2 ×10^5 valves g^{-1} and <3%,

418   respectively). Here, the siliceous assemblage was almost completely conformed by

419   *Chaetoceros* resting spores (RS) (Fig. 7).

420   A total of 135 and 8 diatom taxa were identified in cores BGGC5 and BTGC8

421   respectively, where the core BTGC8 registered very low abundances of diatoms. In

422   general, diatoms were the most important assemblage of siliceous microfossils (96%),

423   followed by sponge spicules (3%). The contribution of phytoliths and chrysophyte cysts

424   was less than 2% in core BGGC5. *Chaetoceros* (RS) dominated the diatom assemblage

425   (~90%; Fig. 7), and included the species *C. radicans*, *C. cinctus*, *C. constrictus*, *C.*

426   *vanheurckii*, *C. coronatus*, *C. diadema*, and *C. debilis*. Other species recorded of

427   upwelling group (mainly in core BGGC5) were: *Skeletonema japonicum,* and

428   *Thalassionema nitzschioides* var. *nitzschioides* (Table S2). Freshwater diatoms

429   (*Diploneis papula, Cymbella tumida, Fragilaria capucina, Diatoma elongatum)* and

430   non-planktonic diatoms (*Cocconeis scutellum*, *C. costata* and *Gramatophora angulosa*)

431   accounted for ~0.1−5%; while the group of coastal planktonic diatoms accounted for

432   ~0.3−6% of the total assemblage. The main planktonic diatoms were (*Rhizosolenia*

433   *imbricata*, and *Thalassiosira eccentrica*). Oceanic-warm diatoms (*Roperia tesselata*,

434   *Th. nitzschioides var inflatula)* and the tycoplanktonic diatom group were rare with less

435   than 1%.

436

4.3.2. TOC and stable isotopes distribution

438   Consistent with opal and diatoms, core BGGC5 showed higher values of TOC

439   (between 2 % and 5 %) compared with less than ~1.5 % in core BTGC8 (Fig. 5a,b).

440   Furthermore, $\delta^{13}C$ was slightly higher at core BTGC8 (-20 ‰ to -21 ‰) compared

441   with core BGGC5 (-21 ‰ to -22 ‰), the former also showing slightly increased

442   values of $\delta^{15}N$ from the deeper sections to the surface of the core (<7 ‰ to >10 ‰).

443   This increase was less evident at core BGGC5, with values of ~9 ‰ at depth to >10 ‰

444   on the surface (Fig. 5a,b). Diminishing TOC contents was related to slightly higher

445    $\delta^{13}C$ values (~ -20 ‰) in both cores.

446

4.3.3. Pollen record

448   Initial surveys on core BTGC8 (Tongoy Bay) revealed extremely low pollen

449   abundances which impeded further palynology work. A complete pollen analysis was

450   only conducted for core BGGC5 (Guanaqueros Bay). The pollen record of core

451   BGGC5 consisted of 29 samples shown in Figure 8. The record was divided in five

452   general zones following visual observation of changes in the main pollen types and

453   also assisted by the cluster analysis CONISS.

454   Zone BG-1 (cal BC 6250 – cal BC 5650): This zone is dominated by the herbaceous

455   taxa Chenopodiaceae, Ast. *Leucheria-type*, Ast. Asteroideae, Apiaceae with relatively

456   high values of the wetland genus *Typha spp*.

457   Zone BG-2 (cal BC 5650 – cal BC 4600): This zone is also dominated by

458   Chenopodiaceae, Ast. *Leucheria-type* and Ast. Asteroideae. In addition, other non-

459   arboreal elements such as Ast. *Ambrosia-type*, Poaceae, Brassicaceae and *Chorizanthe*

460   *spp.* expand notably.

14

461   Zone BG-3 (cal BC 4600 – cal BC 1450): This zone is marked by a steady decline in

462   Chenopodiaceae and Ast. *Leucheria-type*, and by the expansion of several other

463   herbaceous elements, such as Euphorbiaceae, Ast. *Baccharis-type* and Brassicaceae.

464   Zone BG-4 (cal BC 1450 – cal AD 1800): This zone is mostly dominated by Ast.

465   Asteroideae, and marked by the decline of Chenopodiaceae and Ast. *Leucheria-type*.

466   Other coastal taxa such as Euphorbiaceae, Ast. *Baccharis-type*, Ast. Chichorioideae,

467   *Quillaja saponaria*, Brassicaceae and *Salix spp*. also expand in this zone.

468   Zone BG-5 (cal AD 1800 – cal AD 2014): The upper portion of the record is

469   dominated by Ast. Asteroideae and Poaceae, and marked by increments of

470   Geraniaceae, Ast. Mutisieae, Myrtaceae and *Q. saponaria*. Additionally, this zone

471   includes introduced pollen types such as *Rumex* and *Pinus*. The latter is not shown in

472   the diagram of Figure 8 because its abundance was minimal.

473   The most distinctive change revealed in core BGGC-5 is a long-term decrease in

474   Chenopodiaceae and increments in Euphorbiaceae and Ast. Asteroideae. Along with

475   this trend, a later expansion of several other representatives of the coastal shrub land

476   starts at around cal BC 4600.

477

478   **4.4. Trace element distributions**

479   Trace element distributions are shown in figures 6a and 6b for Guanaqueros (BGGC5)

480   and Tongoy Bays (BTGC8), respectively. Trace metals sensitive to the presence of

481   oxygen (U, Re, Mo) showed increasing metal/Al ratios from the base of the core (cal

482   BC ~6300) until cal BC 4500 in core BGGC5. After this maximum, ratios presented a

483   slight increase towards the beginning of the recent era (cal AD 1) followed by a sharp

484   decrease until present. Similarly, the metal ratios in the core BTGC8 increase over

485   time, yet the maximum was observed at cal AD 1000. The exception of this trend was

486   Mo which exhibited maximum values until cal BC 4000 and then a steady decrease

487   towards the present. Additionally, metal/Al values were higher at core BGGC5. Iron

488   displayed a clear increase around cal BC 2000 at core BGGC5, and at core BTGC8

489   was observed a slight increase after cal BC ~3000. Manganese did not show a clear

490   trend.

491   A second element group (metal/Al ratios), including Cd, Ni and P (related to primary

492   productivity and organic fluxes), showed a similar pattern than Mo/Al towards the

493   bottom of core BGGC5, i.e. the highest values around cal BC 4500 and a constant

494   reduction towards the present. A third group, consisting of Ba, P and Ca, exhibited a

495 less clear pattern. The Cd/Al and Ni/Al ratios in core BTGC8 showed only slightly

496 decreasing values, and the maximum values were very low compared to the BGGC5

497 core. The same pattern is observed for other elements. Metal/Al ratios for Ba, Ca and

498 P were lower and presented a long-term decreasing pattern towards the present.

499 An exception to the previously described patterns was Cu/Al, which peaked at cal BC

500 2000 and showed a conspicuous increase in the past ~150 years. This was also

501 observed at core BTGC8, but with lower concentrations than at core BGGC5.

502

503 **5. Discussion**

504 **5.1. Sedimentary composition of the cores: terrestrial *versus* biogenic inputs**

505 The sediments in the southern zones of the bays constitute a sink of fine particles

506 transported from northern areas and the shelf (Fig. 5a, 5b), responding to the water

507 circulation in the Guanaqueros and Coquimbo Bays described as bipolar, i.e. two

508 counter-rotating gyres which are counterclockwise to the north and clockwise to the

509 south (Valle-Levinson and Moraga, 2006). This is the result of the wind and a

510 coastline shape delimited by two prominent points to the north and south. In the case

511 of Tongoy Bay (the southernmost bay of the system), circulation shows a different

512 pattern due to its northern direction compared to Guanaqueros Bay, which opens to the

513 west. The cyclonic recirculation in Tongoy Bay seems to be part of a gyre larger than

514 the Bay's circulation (Moraga et al., 2011). This could explain differences in sediment

515 particle distribution and composition between the bays. At Tongoy Bay, there are less

516 organic carbon accumulation (< 2 %), siliceous microfossils and pollen (Figs. 5, 7 and

517 8). Similarly, in Guanaqueros Bay TOC contents are only slightly higher (> 2 %),

518 especially before cal BC 1000 (~ 4 %). However, sediments there contain enough

519 microfossils to establish differences in primary productivity periods and also provide a

520 pollen record evidencing the prevailing environmental conditions.

521 The stable isotopes measured in the study area were in the range of marine

522 sedimentary particles for southern oceans at low and mid latitudes (δ^{13}C; -20 ‰ – -24

523 ‰; Williams 1970; Rau et al., 1989; Ogrinc et. al. 2005), and slightly lower than the

524 TOC composition at the water column (-18 ‰, Fig. 3). This suggests that the organic

525 particles that settle on the bottom are a more refractory material (C/N: 9−11),

526 remineralized during particle transportation and sedimentation. This results in lighter

527 isotopic compositions, especially at core BTGC8. Besides, the δ^{15}N and δ^{13}C of settled

528 particles are more negative at surface sediments due to a preferential degradation of

16

529   molecules rich in ^{13}C and ^{15}N, resulting in more negative values and higher C/N ratios

530   at sediments than in suspended particles (Fig. 3, 5a, 5b). However, this is also due to

531   the stronger diagenetic reactions observed near the bottom layer (Nakanishi and

532   Minagawa, 2003), indicating that the particles' diagenesis and time of transportation

533   over the shelf should be a relevant factor in this differentiation. Thus, these sediments

534   are composed by winnowed particles transported by water circulating over the shelf,

535   and the isotopic variations should not establish clearly the contribution of terrestrial

536   inputs.

537   Magnetic susceptibility (MS) measurements revealed lower values throughout both

538   cores (BGGC5: 5 – 8 x10^{-8} SI; BTGC8: 12 – 20 x10^{-8} SI), except at dates after ~ cal

539   AD 1800, when the susceptibility increases substantially to values similar to those

540   observed in the Pachingo wetland (40 – ~200 x10^{-8} SI; unpublished data) on the

541   southern side of Tongoy Bay. Magnetite has strong response to magnetic fields and its

542   concentration is considered proportional to magnetic susceptibility (Dearing, 1999).

543   Besides, mineral post-depositional transformations (alteration of magnetite minerals)

544   and dilution by biogenic components (carbonates, silicates) should also be relevant in

545   the MS intensity in zones with high organic accumulation rates (Hatfield and Stoner,

546   2013). However, this is not expected to be the case for our cores and the MS should be

547   mainly accounting for the source of the particles. High MS measurements in the bay

548   sediments would be associated with relevant terrestrial input. The area is surrounded

549   by several creeks that are only active during major flooding events, with greater

550   impacts in Tongoy Bay compared to Guanaqueros Bay. An important increment in the

551   contribution of terrestrial material has occurred in Tongoy Bay in recent times (Ortega

552   et al., in review), which is diluting organic proxy records and increasing the grain size.

553   Our records indicate a slight increase in mean grain size at both bays, supported also

554   by a slight decrease in Ca/Fe ratio indicating more Fe input from continental erosion

555   (Fig. 5a, 5b).

556   Recent information indicates that during the intensification of southern winds the

557   upwelling develops a nutrient-rich and low-oxygen flow within the bay's southern

558   areas (Gallardo et al., 2017), which promotes phytoplankton blooms and low oxygen

559   events. Decreasing concentrations of Ca from the deepest part of both cores to the

560   surface was interpreted as decreasing primary productivity (Keshav and Achyuthan,

561   2015; Sun et al., 2016), but higher concentrations were measured in core BGGC5

562   compared with core BTGC8, where more terrestrial influence is being suggested. The

563   slight increase of K/Ca ratio in time, from bottom to the surface, should also be

564   interpreted as a slight increase in continental input, since K is related to siliciclastic

565   material from coastal erosion, fluvial and groundwater inputs. However, the variation

566   of Ca was larger (Fig.6a, 6b), resulting in higher K/Ca ratios at the surface. This

567   indicating that the continental input has not changed much in time but rather the

568   primary productivity has decreased (Fig. 5a, 5b).

569

5.2. Temporal variability of proxies for primary productivity

571   Several elements participating in phytoplankton growth are useful to interpret

572   variations in primary productivity in time, as they are preserved within the sediments

573   under suboxic-anoxic conditions. This produces enrichment over crustal abundance,

574   which distinguishes them from continental inputs. The presence of free dissolved

575   sulfides produced by sulfate reduction reactions in the diagenesis of organic matter is

576   relevant for metal precipitation in pore water (Calvert and Pedersen, 1993; Morse and

577   Luther, 1999). At the same time, organic matter remineralization releases ions to the

578   pore water where they could form organic complexes and insoluble metal sulfides.

579   Conversely, they could be incorporated into pyrite as Cd, Ni and Cu, showing

580   different degrees of trace metal pyritization (Huerta-Diaz and Morse, 1992). Ca, Sr,

581   Cd and Ni profiles suggest a lower proportion of organic deposition in time (Fig. 6a,

582   6b), consistent with the slight reduction of TOC content in time observed in the

583   sediments (Figs. 5a, 5b), and concomitantly with other elements related to organic

584   fluxes to the bottom and primary productivity. In the case of Ba, it is actively

585   incorporated into phytoplankton biomass or adsorbed onto Fe oxyhydroxides,

586   increasing the Ba flux towards the sediments, where it is also released during organic

587   matter diagenesis. Ba is precipitating in microenvironments where Ba-sulfate reaches

588   supersaturation (Tribovillard et al., 2006 and references therein), but it is dissolved in

589   suboxic-anoxic environments or where sulfate is significantly depleted (Torres et al.,

590   1996; Dymond et al., 1992). Therefore, it is better preserved in less anoxic

591   environments with moderate productivity, expected to be the case of our study site

592   (Gross Primary Productivity =0.35 to 2.9 g C $m^{-1}d^{-1}$; Daneri et al., 2000). Hence, the

593   slight increase of Ba from cal BC 4000 (Fig. 6a) to the present should rather be the

594   response to a less anoxic environment than to an increase in primary productivity. This

595   is consistent with the reduction in TOC and other nutrient-type elements (Ni, Sr, Ca,

596   Cd), and results in a low negative correlation with TOC (-0.59; Table 4) due to the Ba

597   remobilization in anoxic conditions after high organic material deposition during cal

598   BC 4000−4500. On the other hand, P distribution showed a trend similar to that of

599   TOC and other elements related to organic fluxes to the bottom, although with a lower

600   correlation. The accumulation of P depends on the deposition rate of organic P (dead

601   plankton, bones and fish scales) to the bottom, and is actively remineralized during

602   aerobic or anaerobic bacterial activity. Dissolved P diffuses towards the water column

603   where part of it could be adsorbed onto Fe oxides that maintain this element within the

604   sediments. P is buried during a continued sedimentation process and could be released

605   to the pore water under anoxic conditions, when oxides are reduced, creating the

606   environmental conditions for phosphorite and carbonate-fluorapatite precipitation.

607   Normally, this takes place in sites with high sedimentation rates and high organic

608   matter fluxes to the bottom (Filippelli, 1997; Cha et al., 2005), which was not the case

609   for our study area (<0.02 cm yr^{-1}). In spite of this difference, P and TOC showed a

610   decreasing trend towards the present, suggesting reducing flux of organic matter over

611   time, which was also observed for Ni and Cd distributions. Alternatively, it could be

612   explained by the increased remineralization of the organic material settled on the

613   bottom (Figs. 6a, 6b).

614   Productivity reconstructions were based on diatom relative abundances and biogenic

615   opal content only in core BGGC5, since core BTGC8 registered valve counts that

616   were too low ($<1\%$ in relative diatom abundance). However, at both cores diatom

617   assemblages were represented mainly by *Chaetoceros resting spores*, which are used

618   as upwelling indicators, showing increased concentrations during periods of high

619   productivity and upwelling (Abrantes 1988, Vargas et al., 2004). In addition,

620   *Chaetoceros* resting spores are highly silicified and well preserved in coastal

621   sediments (Blasco et al., 1981). The downcore siliceous productivity based on opal

622   distribution (Fig. 7) distinguished three main periods of increased productivity: (1)

623   recent time cal AD 2014 – cal AD ~1800, (2) cal AD 1 – cal BC 2300 and (3) > cal

624   BC 4300. The mean opal accumulation rate in the second period was 11.8 ± 4.8 g m^2

625   yr^{-1}, when spicules and minerals (quarz, framboid pyrite) where abundant in smear

626   slides. During the third period, accumulation increased highly to ~30.1 ± 14.5 g m^2 yr^{-}

627   ^{1}, when the *Chaetoceros* spores were predominant, indicating upwelling intensification

628   and low spicules and minerals were observed in the slides. This is partially consistent

629   with the nutrient–type element distributions. Although the first period was too short,

630   high opal accumulation and high Cd/U ratios could also be observed, which increased

631   toward the present (mean opal value of 32.3 ± 22.4 g m^2 yr^{-1}). Similarly, Cu and Fe

632   also increased in recent times (Fig. 6a), contributing to fertilize the environment and

633   promoting primary productivity. The second period was not clearly identified in terms

634   of metals, except for Fe which shows a conspicuous increment in this period (Fig. 6a).

635   During the third period, all metal proxies showed primary productivity increases

636   before cal BC 4500, as indicated by opal accumulation within the sediments. In

637   anoxic-suboxic environments Cd/U ratios could vary between 0.2 and 2 (Nameroff et

638   al., 2002), the high concentrations of both elements reflect anoxic conditions but their

639   different behavior could result in variable Cd/U ratios in suboxic environments. Here,

640   the Cd and U accumulation on sediments resulted in high Cd/U ratios (>2; Fig. 7)

641   during periods with high opal accumulation in the cores, especially in the third period,

642   and even in core BTGC8; and lower ratios (< 1; Fig. 7) when opal was low, indicating

643   higher variations in the primary productivity in time with moderated changes in

644   oxygen conditions at the bottoms. Opal showed good correlations with Ni and Cd

645   (˜0.70; Table 4; Fig. 6a), all suggesting the relevance of bottom organic fluxes for

646   element accumulation within the sediments, and establishing a clear period of higher

647   primary productivity around cal BC 4500, when lowest oxygen conditions prevailed

648   (Fig. 7).

649

650   **5.3. Temporal variability of proxies for bottom water oxygenation**

651   U, Re and Mo distributions in core BGGC5 indicate that anoxic or suboxic conditions

652   were developed from cal BC 6000 to ~ cal AD 1−1000. After this period and towards

653   the present, however, a remarkable reduction in their concentration suggests a more

654   oxygenated bottom environment, concurrent with lower organic fluxes to the

655   sediments. The Re profile shows the influence of suboxic waters not necessarily

656   associated with increased organic matter fluxes to the bottom. Since this element is not

657   scavenged by organic particles, its variability is directly related to oxygen changes

658   (Calvert and Pedersen, 2007, and references therein). Additionally, it is strongly

659   enriched above crustal abundance in suboxic conditions (Colodner et al., 1993;

660   Crusius et al 1996), being >10 times in core BGGC5 (Fig. 9) before cal AD 1. In the

661   same way, U exhibits a similar pattern, and although organic deposition has an impact

662   on its distribution (Zheng et al., 2002), it also relates to changes in bottom oxygen

663   conditions. This is because its shift from a soluble conservative behavior to non-

664   conservative and insoluble solely depends on the redox potential change that occurs

665   near the Fe(III) reduction zone (Klinkhammer and Palmer, 1991). Molybdenum,

666   which showed high increases at cal BC 4500, also indicates the presence of sulfidic

667   conditions, as shown by the Re distribution highly enriched in anoxic environments

668   (Colodner et al., 1993), and by the reduction of Re(VII) to Re(IV) forming ReO_2 or

669   ReS (Calvert and Pedersen, 2007). Rhenium, U and Mo enrichment is relevant to

670   decipher the redox condition within the sediments, even in places with high lithogenic

671   input that could obscure the authigenic enrichment of other elements under similar

672   conditions (Crusius et al., 1996). In both places, the concentrations of these elements

673   showed values above the crustal abundance, especially in core BGGC5 (Fig. 9), with

674   Re and Mo becoming more enriched than U. This suggests that the presence of anoxic

675   conditions were stronger around cal BC 4500−5000. The most relevant enrichment

676   was observed for Cd (> 30, Fig 9), which could similarly indicate the sulfidic

677   condition within the sediments that allows Cd precipitation. It is also supported by Mo

678   enrichment, since its accumulation within the sediments is highly controlled by sulfide

679   concentrations (Chaillou et al., 2002; Nameroff et al., 2002; Sundby et al., 2004).

680   Something similar occurs in Tongoy Bay (core BTGC8), but trace metal

681   concentrations are lower for all elements and also for TOC, suggesting that it has

682   limited influence on metal accumulation within the sediments. Thus, these elements

683   suggest anoxic conditions within the sediments in both places around cal BC

684   4500−5000 (Fig. 6a, 6b). After this period, a second maximum but less intense anoxia

685   is observed at the beginning of the recent era (cal AD 1−1000), continuing with a

686   conspicuous oxygenation until present times. This interpretation based on the

687   distribution of U, Re and Mo complements the observations of nutrient-type elements

688   pointing both to oxygenation changes in time and to changes in organic fluxes to the

689   sediments. A less prominent accumulation of nutrient-type elements (Ni, Cd, Ba, Ca

690   and P) would indicate lower organic material deposition to the sediments but

691   promoting anoxic conditions within the sediments and lower sulfide content with time,

692   which are nevertheless high enough to sustain Mo accumulation until cal AD 1. After

693   that, a notorious decrease in Re, U and Mo accumulation was observed, suggesting

694   that the oxygenation of the bottom becomes relevant. This could also explain the

695   conspicuous increase of Cu/Al and Fe/Al in recent times due to the presence of oxides

696   (Fig. 6a, 6b). Apparently, a low level of dissolved Cu is maintained by the

697   complexation with organic compounds produced by phytoplankton and Cu adsorption

698   on Fe oxides (Peacock and Sherman, 2004; Vance et al., 2008; Little et al., 2014), with

21

699 both processes increasing Cu in the particulate phase over surface sediments. At our

700 study sites, Fe and Cu concentrations were higher in surface sediments, probably

701 related to an increase in Fe and Cu availability in the environment (Fig 6a, 6b). This

702 could be in turn associated with mining activities carried out in the area since the

703 beginning of cal AD 1900's. At present, the suboxic conditions within the bays result

704 from the influence of adjacent water masses with low oxygen contents, related to the

705 oxygen minimum zone (OMZ) (Fig. 2) centered at ~250 m. Upwelling promotes the

706 intrusion of these waters towards the bays, with strong seasonality. Transition times

707 develop in short periods by changes in wind directions and intensities along the coast.

708 Additionally, oceanic variability along the western coast of South America is influenced by

709 equatorial Kelvin waves on a variety of timescales, from intraseasonal (Shaffer et al.,1997)

710 and seasonal (Pizarro et al., 2002; Ramos et al., 2006) to interannual (Pizarro et al., 2002;

711 Ramos et al., 2008). Coastal-trapped Kelvin waves originating from the equator can propagate

712 along the coast, modify the stability of the regional current system and the pycnocline, and

713 trigger extratropical Rossby waves (Pizarro et al., 2002; Ramos et al., 2006; 2008). This

714 oceanographic feature will generate changes in oxygen content within the bays with

715 major impacts on redox sensitive elements in surface sediments; thus, the increased

716 frequency and intensity of this variability would result in a mean effect which is

717 observed as a gradual change in metal contents in time.

718

5.6. Climatic interpretations

720 Past environmental changes are analogue with the present seasonal meridional

721 displacement of the ITCZ (Intertropical Convergence Zone) and SPSH (South Pacific

722 Subtropical High) expansion/contraction, establishing cold-dry/warm-humid climate

723 conditions ('winter like/summer like') (Hebbeln et al., 2002; Lamy et al., 2001, 2002,

724 2010). In this regard, the Holocene climate of the semi-arid zone of Chile has alternated

725 between wet and dry phases, associated with the intensity and latitudinal position of the

726 Southern Westerly Wind belt (SWW). Studies based on pollen records in southern

727 coastal areas of Coquimbo (30°S) indicate that wet conditions were predominant before

728 cal BC 6750, which brought the expansion of swamp forests areas along the coast. This

729 wet period was followed by a long-lasting arid phase that culminated in peak dry

730 conditions at cal BC 5550–3750 (Maldonado and Villagrán, 2006; Maldonado and

731 Rozas, 2008). This timing matches the relative dry conditions detected in the first

732 portion of our pollen reconstruction, indicated by relative low values of the Pollen

Biogeosciences
Discussions

733   Moisture Index (Fig. 10). Our results further suggest that these dry conditions were

734   followed by trends towards increasing precipitation from the mid-Holocene onwards

735   (from cal BC ~4500 to ~ cal AD 1800), as indicated by the increasing values in the

736   Pollen Moisture Index and continental runoff (Fig. 10). Al and Pb are considered

737   indicators of continental particle inputs to marine waters transported mainly by river

738   runoff and dust (Saito et al 1992; Calvert and Pedersen, 2007; Govin et al., 2012; Xu et

739   al. 2015; Ohnemus and Lam, 2015). In our cores, these elements showed a trend similar

740   to pollen, i.e., a gradual rise in time, suggesting increased humid conditions during

741   recent periods. Therefore, this pattern of humidity and continental influence variability

742   in Guanaqueros Bay sediments suggests an increase in winter rainfall or an increased

743   frequency of episodic rainfall events since ~250 Cal BC (Ortega et al., submitted).

744   South of 35°S, an overall strengthening of SWW and a poleward shift driven by orbital

745   forcings seem to be operating from the mid-Holocene (7 kyr BP) to pre-industrial

746   modern times (250 yr BP) (Varma et al., 2012), promoting more humid conditions in

747   this period. Our records indicates increases in grain size, K/Ca ratios, and Fe and Al

748   contents over time, all of which point to higher continental inputs, most probably by

749   increasing rainfall events, which should be an important source of Fe in northern

750   Chilean margin, related to primary productivity increases in sedimentary records

751   (Dezileau et al., 2004). This study shows slight increases in Fe concentrations at cal BC

752   ~1500−2000 and at cal BC ~4000; both periods showing clear increases in primary

753   productivity. However, maximum productivity observed at cal BC ~4000 –interpreted

754   from the accumulation of nutrient type elements, and the distribution of opal and

755   diatoms– was consistent with overall dry environmental conditions (Fig. 6, 8), also

756   connected to an anoxic sulfidic environment. This could be related to an increased

757   intensity of the anticyclone and a consequently higher upwelling during this period

758   (Frugone-Álvarez et al., 2017).

759   Peak drying with higher productivity and lower oxygen conditions was followed by a

760   gradually decreasing primary productivity and organic fluxes. The maximum

761   productivity occurred during the driest period studied (mid-Holocene), suggesting

762   stronger upwelling that was weakening in time concomitantly with the increase of

763   humid conditions. In this case, weakened upwelling could be interpreted as an intrusion

764   of less nutrient-enriched upwelled waters over the shelf, influenced by remote equatorial

765   waves as observed today. Normally, the wet/dry phases associated with ENSO-like

766   conditions also influence bottom oxygenation which has been observed from the central

23

767   Peruvian coast to the southern Chilean regions (12 °S − 36 °S) (Escribano et al., 2004;

768   Gutiérrez et al., 2008); thus, OMZ is expected to be less/more intense during warm/cold

769   phases. Besides, the Walker circulation strength and the expansion/contraction of the

770   SPSH also control marine productivity (Salvatteci et al., 2014), a key variable closely

771   related to the supply of nutrient rich and poor oxygen waters belonging to the OMZ.

772   Thus, warm periods tend to be associated with low productivity and weak OMZ

773   (Salvatteci et al., 2014). In this sense, an increase in the frequency of ENSO-like warm

774   periods influences bottom oxygenation, resulting in a less reduced environment

775   concomitantly with less organic fluxes from primary productivity and less oxygen

776   consumption during organic matter diagenesis.

777

778   **6. Conclusions**

779   The circulation seems to affect both places differently, leaving more variable grain

780   compositions and higher TOC contents in the Guanaqueros Bay (core BGGC5) than in

781   the Tongoy Bay (core BTGC8). This difference should be interpreted as an increase in

782   the time of particle transportation resulting in grain size selection (more leptokurtic at

783   core BTGC8), especially after cal AD 1. Furthermore, in both bays, constantly

784   decreasing TOC contents were observed after cal BC ~2000 to the present, probably

785   due to higher oxygenation of the bay bottom in time.

786   In the investigated sediments, differences in redox conditions could be reconstructed

787   showing a clear decreasing trend in oxygen bottoms before the beginning of recent

788   time (cal AD 1), followed by a rapid change to a more oxygenated environment in the

789   last 2000 years. The environmental conditions at bottom waters were relevant in the

790   metal enrichment factor above crustal abundance within the sediments (highest EFs),

791   since low organic carbon accumulation and low sedimentation rates have been

792   estimated, indicating that the accumulation of these elements (U, Mo and Re) depends

793   mainly on oxygen content instead of on organic carbon burial rates. Apparently, a

794   maximum suboxia-anoxia occurred at cal BC ~4500 year BC, when peak U and Re

795   where recorded, probably due to the presence of a sulfidic environment.

796   The nutrient-type elements follow a similar trend, reduced at present and showing

797   higher accumulation rates around cal BC 4500 (Ca, Ni, P and Cd). Their distribution is

798   consistent with the diatom and opal distributions, showing their dependence on primary

799   productivity and organic carbon burial rates. If the kinetics reaction is working at low

800   rates for these elements, they should be highly influenced during oxygenation periods,

801   something that seems to have been operating with higher frequencies.

802   The record of continental proxies establishes a continuous increment in wet

803   conditions, consistent with previous reconstructions in central Chile. The most

804   distinctive changes were observed after cal BC 4500, when an overall expansion of the

805   coastal vegetation occurred as a result of a progressive increase in precipitation and

806   river runoffs, expanding the grain size of the sediments and the increase

807   concentrations of elements that has relevant continental source (Al, Fe, K and Pb).

808   Increased regional precipitations amounts have been commonly interpreted by a

809   northward movement of the Southern Westerly Winds belts, but the increased

810   frequency of El Niño events have also introduced a high variability of humidity in the

811   late Holocene. Thus, the apparent increase of oxygen conditions at bottoms would be

812   the result of this oceanographic feature, which introduced a more oxygenated water

813   mass to the shelf and bays, temporarily changing the redox conditions in surface

814   sediments and affecting the sensitive elements to redox potential change in the

815   environment. Additionally, this also affected the accumulation of organic matter due

816   to an intensification of its remineralization, showing a decreasing trend in nutrient type

817   element accumulation and organic carbon burial rates towards the present.

818

819   **7. References**

820   Abrantes, F.: Diatom assemblages as upwelling indicators in surface sediments off

821   Portugal, Mar. Geol., 85(1), 15–39, doi:10.1016/0025-3227(88)90082-5, 1988.

822

823   Appleby, P. G. and Oldfield, F.: The calculation of lead-210 dates assuming a constant

824   rate of supply of unsupported210Pb to the sediment, Catena, 5(1), 1–8,

825   doi:10.1016/S0341-8162(78)80002-2, 1978.

826

827   Behrenfeld, M. J., O'Malley, R. T., Siegel, D. A., McClain, C. R., Sarmiento, J. L.,

828   Feldman, G. C., Milligan, A. J., Falkowski, P. G., Letelier, R. M. and Boss, E. S.:

829   Climate-driven trends in contemporary ocean productivity, Nature, 444(7120), 752–

830   755, doi:10.1038/nature05317, 2006.

831

832   Bevington, P. and Robinson, K. (Eds.): Error analysis. In: Data Reduction and Error

833   Analysis for the Physical Sciences, WCB/McGraw-Hill, USA, 38–52, 1992

834

835 Blasco, D., Estrada, M. and Jones, B. H.: Short time variability of phytoplankton

836 populations in upwelling regions-the example of Northwest Africa. In: Coastal

837 upwelling. F. A. Richards (Ed.), AGU Washington DC, 339 – 347, 1981

838

839 Blott, S. J. and Pye, K.: Gradistat: A Grain Size Distribution and Statistics Package for

840 the Analysis of Unconcolidated Sediments, Earth Surf. Process. Landforms, 26, 1237–

841 1248, doi:10.1002/esp.261, 2001.

842

843 Bolin, B.: The carbon cycle and global change: a focus on CO2. In: Trace Gases and the

844 Biosphere. Moore, B. III and Schimel, D. (Eds.), Boulder: University Corporation for

845 Atmospheric Research, 129−149, 1992.

846

847 Calvert, S. E. and Pedersen, T. F.: Geochemistry of Recent oxic and anoxic marine

848 sediments: Implications for the geological record, Mar. Geol., 113(1–2), 67–88,

849 doi:10.1016/0025-3227(93)90150-T, 1993.

850

851 Calvert, S. E. and Pedersen, T. F.: Chapter Fourteen Elemental Proxies for

852 Palaeoclimatic and Palaeoceanographic Variability in Marine Sediments: Interpretation

853 and Application, Dev. Mar. Geol., 1(7), 567–644, doi:10.1016/S1572-5480(07)01019-6,

854 2007.

855

856 Cha, H. J., Lee, C. B., Kim, B. S., Choi, M. S. and Ruttenberg, K. C.: Early diagenetic

857 redistribution and burial of phosphorus in the sediments of the southwestern East Sea

858 (Japan Sea), Mar. Geol., 216(3), 127–143, doi:10.1016/j.margeo.2005.02.001, 2005.

859

860 Chaillou, G., Anschutz, P., Lavaux, G., Schäfer, J. and Blanc, G.: The distribution of

861 Mo, U, and Cd in relation to major redox species in muddy sediments of the Bay of

862 Biscay, Mar. Chem., 80(1), 41−59, doi:10.1016/S0304-4203(02)00097-X, 2002.

863

864 Chester, R.: Redox environments and diagenesis in marine sediments, In: Marine

865 Geochemistry, Chapman & Hall, 486−524, 1990.

866

867   Colodner, D., Sachs, J., Ravizza, G., Turekian, K. K. and Boyle, E.: The geochemical

868   cycle of Re: a reconnaissance, Earth Planet. Sci. Lett., 117, 205–221, doi:10.1016/0012-

869   821X(93)90127-U, 1993.

870

871   Crusius, J., Calvert, S., Pedersen, T. and Sage, D.: Rhenium and molybdenum

872   enrichments in sediments as indicators of oxic, suboxic and sulfidic conditions of

873   deposition, Earth Planet. Sci. Lett., 145(1–4), 65–78, doi:10.1016/S0012-

874   821X(96)00204-X, 1996.

875

876   Cupp, E.E.: Marine plankton diatoms of the west coast of North America, Bulletin of

877   the Scripps Institution of Oceanography 5, 1–238, 1943.

878

879   Daneri, G., Dellarossa, V., Quiñones, R., Jacob, B., Montero, P. and Ulloa, O.: Primary

880   production and community respiration in the Humboldt Current System off Chile and

881   associated oceanic areas, Mar. Ecol. Prog. Ser., 197, 41–49, doi:10.3354/meps197041,

882   2000.

883

884   Dearing, J., Magnetic susceptibility. In: Environmental Magnetism: A Practical Guide.

885   Walden, J., Oldfield, F., and Smith, J. (Eds.), Quaternary Research Association

886   Technical Guide No. 6, London, 35–62, 1999.

887

888   Dymond, J., Suess, E. and Lyle, M.: Barium in deep-sea sediment: A geochemical

889   proxy for paleoproductivity, Paleoceanography, 7(2), 163−181, 1992.

890

891   Dezileau, L., Ulloa, O., Hebbeln, D., Lamy, F., Reyss, J. L. and Fontugne, M.: Iron

892   control of past productivity in the coastal upwelling system off the Atacama Desert,

893   Chile, Paleoceanography, 19(3), doi:10.1029/2004PA001006, 2004.

894

895   Escribano, R., Daneri, G., Farías, L., Gallardo, V. A., González, H. E., Gutiérrez, D.,

896   Lange, C. B., Morales, C. E., Pizarro, O., Ulloa, O. and Braun, M.: Biological and

897   chemical consequences of the 1997-1998 El Niño in the Chilean coastal upwelling

898   system: A synthesis, Deep. Res. Part II Top. Stud. Oceanogr., 51(20–21), 2389–2411,

899   doi:10.1016/j.dsr2.2004.08.011, 2004.

900

901 Faegri, K. and Iversen, J.: Textbook of pollen analysis, IV. The Blackburn Press, New

902 Yersey, 328 pp., 1989.

903

904 Filippelli, G. M.: Controls on phosphorus concentration and accumulation in oceanic

905 sediments, Mar. Geol., 139, 231-240, 1997.

906

907 Flynn, W. W.: The determination of low levels of polonium-210 in environmental

908 materials, Anal. Chim. Acta, 43, 221–227, 1968.

909

910 Frugone-Álvarez, M., Latorre, C., Giralt, S., Polanco-Martínez, J., Bernárdez, P., Oliva-

911 Urcia, B., Maldonado, A., Carrevedo, M. L., Moreno, A., Delgado Huertas, A., Prego,

912 R., Barreiro-Lostres, F. and Valero-Garcés, B.: A 7000-year high-resolution lake

913 sediment record from coastal central Chile (Lago Vichuquén, 34°S): implications for

914 past sea level and environmental variability, J. Quat. Sci., 32(6), 830–844,

915 doi:10.1002/jqs.2936, 2017.

916

917 Gallardo, M.A., González, A., Ramos, M., Mujica, A., Muñoz, P., Sellanes, J.,

918 Yannicelli, B.: Reproductive patterns in demersal crustaceans from the upper boundary

919 of the OMZ off north-central Chile, Cont. Shelf. Res. 141, 26–37, 2017.

920 http://dx.doi.org/10.1016/j.csr.2017.04.011

921

922 Garreaud, R. and Rutllant, J.: Análisis meteorológico de los aluviones de Antofagasta y

923 Santiago de Chile en el período 1991–1993, Atmósfera, 9, 251–271, 1996.

924

925 Garreaud, R., Vuille. M., Compagnuccic, R. and Marengo, J.: Present-day South

926 American climate, Palaeogeogr. Palaeocl., 281, 180-195,

927 doi:10.1016/j.palaeo.2007.10.032

928

929 González, H. E., Daneri, G., Figueroa, D., Iriarte, J., Lefèvre, N., Pizarro, G., Quiñones,

930 R., Sobarzo, M. and Troncoso, A.: Producción primaria y su destino en la trama trófica

931 pelágica y océano profundo e intercambio océano-atmósfera de CO_2 en la zona norte de

932 la Corriente de Humboldt (23º S): posibles efectos del evento El Niño 1997. Rev. Chil.

933 Hist. Nat., 71, 429-458, 1998.

934

935 Govin, A., Holzwarth, U., Heslop, D., Ford Keeling, L., Zabel, M., Mulitza, S., Collins,

936 J. A. and Chiessi, C. M.: Distribution of major elements in Atlantic surface sediments

937 (36°N-49°S): Imprint of terrigenous input and continental weathering, Geochemistry,

938 Geophys. Geosystems, 13(1), 1–23, doi:10.1029/2011GC003785, 2012.

939

940 Guieu, C., Martin, J. M., Tankéré, S. P. C., Mousty, F., Trincherini, P., Bazot, M., Dai,

941 M. H.: On trace metal geochemistry in the western Black Sea: Danube and shelf area.

942 Estuarine, Coastal and Shelf Science, 47, 471–485, 1998.

943

944 Gutiérrez, D., Enríquez, E., Purca, S., Quipuzcoa, L., Marquina, R., Flores, G. and

945 Graco, M.: Oxygenation episodes on the continental shelf of central Peru: Remote

946 forcing and benthic ecosystem response. Prog. Oceanogr., 79, 177–189, 2008.

947

948 Hansen, H. P., Koroleff, F.: Determination of nutrients. In Methods of Seawater

949 Analysis. Grasshoff, K., Kremling, K. and Ehrhardt, M. (Eds.), Wiley-VCH Verlag

950 GmbH, Weinheim, Germany, 159–228, 1999.

951

952 Hatfield, R. G., Stoner, J. S.: Magnetic Proxies and Susceptibility. In: The Encyclopedia

953 of Quaternary Science. Elias, S.A. (ed.) 2, 884-898, 2013.

954

955 Hebbeln, D., Marchant, M. and Wefer, G.: Paleoproductivity in the southern Peru ^

956 Chile Current through the last 33 000 yr, Mar. Geol., 186, 2002.

957

958 Helly, J. and Levin. L.: Global distribution of naturally occurring marine hypoxia on

959 continental margin, Deep-Sea Res. Pt. I, 51, 1159-1168, 2004.

960

961 Heusser, C. J. and Moar, N. T.: Pollen and spores of chile: Modern types of the

962 pteridophyta, gymnospermae, and angiospermae, New Zeal. J. Bot., 11(2), 389–391,

963 doi:10.1080/0028825X.1973.10430287, 1973.

964

965 Huerta-Diaz, M. A. and Morse, J. W.: Pyritization of trace metals in anoxic marine

966 sediments, Geochim. Cosmochim. Acta, 56(7), 2681–2702, doi:10.1016/0016-

967 7037(92)90353-K, 1992.

968

969   Jöris, O. and Weninger, B.: Extension of the C-14 calibration curve to ca. 40,000 cal BC

970   by synchronizing Greenland O-18/O-16 ice core records and North Atlantic

971   foraminifera profiles: A comparison with U/Th coral data, Radiocarbon, 40(1), 495–

972   504, doi:10.2458/azu_js_rc.40.2036, 1998.

973

974   Keshav, N. and Achyuthan, H.: Late Holocene continental shelf sediments, off

975   Cuddalore, East coast, Bay of Bengal, India: Geochemical implications for source-area

976   weathering and provenance, Quat. Int., 371, 209–218, doi:10.1016/j.quaint.2015.03.002,

977   2015.

978

979   Klinkhammer, G. P. and Palmer, M. R. Uranium in the oceans: Where it goes and why,

980   Geochim. Cosmochim. Ac., 55(7), 1799–1806, doi: 10.1016/0016-037(91)90024-Y,

981   1991.

982

983   Lamy, F., Hebbeln, D., Röhl, U. and Wefer, G.: Holocene rainfall variability in southern

984   Chile: a marine record of latitudinal shifts of the Southern Westerlies. Earth Planet. Sc.

985   Lett., 185, 369–382, 2001.

986

987   Lamy, F., Rühlemann, C., Hebbeln, D. and Wefer, G.: High- and low-latitude climate

988   control on the position of the southern Peru-Chile Current during the Holocene,

989   Paleoceanography, 17(2), 16-1-16–10, doi:10.1029/2001PA000727, 2002.

990

991   Lamy, F., Kilian, R., Arz, H.W., Francois J-P., Kaiser, J.,Prange, M. and Steinke, T.:

992   Holocene changes in the position and intensity of the southern westerly wind belt, Nat.

993   Geosci., 3, 695–699, 2010.

994

995   Little, S. H., Vance, D., Walker-Brown, C. and Landing, W. M.: The oceanic mass

996   balance of copper and zinc isotopes, investigated by analysis of their inputs, and outputs

997   to ferromanganese oxide sediments, Geochim. Cosmochim. Acta, 125, 673–693,

998   doi:10.1016/j.gca.2013.07.046, 2014.

999

1000   Maldonado, A. and Rozas, E.: Clima y Paleoambientes durante el Cuaternario Tardío en

1001   la Región de Atacama, in Libro Rojo de la Flora Nativa y de los Sitios Prioritarios para

1002   su Conservación: Región de Atacama, pp. 293–304., 2008.

1003

1004 Maldonado, A. and Villagrán, C.: Climate variability over the last 9900 cal yr BP from

1005 a swamp forest pollen record along the semiarid coast of Chile, Quat. Res., 66(2), 246–

1006 258, doi:10.1016/j.yqres.2006.04.003, 2006.

1007

1008 Marchant, M., Hebbeln, D. and Wefer, G.: High resolution foraminiferal record of the

1009 last 13,300 yeras from the upwelling area off Chile, Mar. Geol., 161, 115–128,

1010 doi:https://doi.org/10.1016/S0025-3227(99)00041-9, 1999.

1011

1012 Marín, V. H., Delgado, L. E. and Luna-Jorquera, G.: S-chlorophyll squirts at 30°S off

1013 the Chilean coast (eastern South Pacific): Feature-tracking analysis. J. Geophys. Res.,

1014 108(12), 3378 – 3384, doi:10.1029/2003JC001935, 2003.

1015

1016 Mazzullo, J., Gilbert, A., Rabinowitz, P., Meyer, A. and Garrison, L.: Handbook for

1017 Shipboard Sedimentologists, 67 pp., 1988.

1018

1019 McManus, J., Nägler, T. F., Siebert, C., Wheat, C. G. and Hammond, D. E.: Oceanic

1020 molybdenum isotope fractionation: Diagenesis and hydrothermal ridge-flank alteration.

1021 Geochem. Geophy. Geosy., 3(12), 1–9, 2002.

1022

1023 Montecinos, A., and Aceituno, P.: Seasonality of the ENSO-Related Rainfall Variability

1024 in Central Chile and Associated Circulation Anomalies. J. Climate., 16, 281–296.

1025 https://doi.org/10.1175/1520-0442(2003)016<0281:SOTERR>2.0.CO;2, 2003.

1026

1027 Montecinos, S., Gutiérrez, J. R., López-Cortés, F. and López, D.: Climatic

1028 characteristics of the semi-arid Coquimbo Region in Chile, J. Arid Environ., 126, 7–11,

1029 doi:10.1016/j.jaridenv.2015.09.018, 2015.

1030

1031 Moraga-Opazo, J., Valle-Levinson, A., Ramos, M. and Pizarro-Koch, M.: Upwelling-

1032 Triggered near-geostrophic recirculation in an equatorward facing embayment, Cont.

1033 Shelf Res., 31, 1991–1999, 2011.

1034

1035   Mortlock, R. A. and Froelich, P. N.: A simple method for the rapid determination of

1036   biogenic opal in pelagic marine sediments, Deep Sea Res. Part A, Oceanogr. Res. Pap.,

1037   36(9), 1415–1426, doi:10.1016/0198-0149(89)90092-7, 1989.

1038

1039   Mosley-Thompson, E., Thompson, L. G. and Lin, P. N.: A multi-century ice-core

1040   perspective on 20th-century climate change with new contributions from high-Arctic

1041   and Greenland (PARCA) cores, Ann. Glaciol., 43, 42–48,

1042   doi:10.3189/172756406781812401, 2006.

1043

1044   Morse, J.W. and Luther, G.W.: Chemical influences on trace metal–sulfide interactions

1045   in anoxic sediments. Geochim Cosmochim Ac., 63, 3373–3378, 1999.

1046

1047   Muñoz, P., Dezileau, L., Cardenas, L., Sellanes, J., Lange, C.B., Inostroza, J., Muratli,

1048   J. and Salamanca, M.A.: Geochemistry of trace metals in shelf sediments affected by

1049   seasonal and permanent low oxygen conditions off central Chile, SE Pacific (~36°S).,

1050   Cont. Shelf Res., 33, 51–68, 2012.

1051

1052   Nakanishi, T. and Minagawa, M.: Stable carbon and nitrogen isotopic compositions of

1053   sinking particles in the northeast Japan Sea, Geochem. J., 37(2), 261–275,

1054   doi:https://doi.org/10.2343/geochemj.37.261, 2003.

1055

1056   Nameroff, T., Balistrieri, L. and Murray, W.: Suboxic trace metals geochemistry in the

1057   eastern tropical North Pacific, Geochim Cosmochim Ac., 66(7), 1139–1158, 2002.

1058

1059   Nurhati, I. S., Cobb, K. M., Charles, C. D. and Dunbar, R. B.: Late 20th century

1060   warming and freshening in the central tropical Pacific, Geophys. Res. Lett., 36(21), 2–5,

1061   doi:10.1029/2009GL040270, 2009.

1062

1063   Ogrinc, N., Fontolan, G., Faganeli, J. and Covelli, S.: Carbon and nitrogen isotope

1064   compositions of organic matter in coastal marine sediments (the Gulf of Trieste, N

1065   Adriatic Sea): indicators of sources and preservation, Mar. Chem., 95, 163-181, 2005.

1066

1067   Ohnemus, D. C. and Lam, P. J.: Cycling of lithogenic marine particles in the US

1068   GEOTRACES North Atlantic transect, Deep. Res. Part II Top. Stud. Oceanogr., 116,

1069   283–302, doi:10.1016/j.dsr2.2014.11.019, 2015.

1070

1071   Paytan, A.: Ocean paleoproductivity, Encyclopedia of Paleoclimatology and Ancient

1072   Environments, Encyclopedia of Earth Science Series, Gornitz, V. (Ed.), Kluwer

1073   Academic Publishers. 2008.

1074

1075   Peacock, C.L. and Sherman, D.M.: Copper(II) sorption onto goethite, hematite and

1076   lepidocrocite: a surface complexation model based on ab initio molecular geometries

1077   and EXAFS spectroscopy. Geochim. Cosmochim. Ac., 68, 2623–2637, 2004.

1078

1079   Pizarro, O., Shaffer, G., Dewitte, B. and Ramos, M.: Dynamics of seasonal and

1080   interannual variability of the Peru-Chile Undercurrent, Geophys. Res. Lett., 29(12), 28–

1081   31, doi:10.1029/2002GL014790, 2002.

1082

1083   Ramos, M., Pizarro,O., Bravo, L. and Dewitte, B.: Seasonal variability of the permanent

1084   thermocline off northern Chile, Geophys. Res. Lett., 33, L09608,

1085   doi:10.1029/2006GL025882, 2006.

1086

1087   Ramos, M., Dewitte, B., Pizarro, O. and Garric, G.: Vertical propagation of

1088   extratropical Rossby waves during the 1997–1998 El Niño off the west coast of South

1089   America in a medium-resolution OGCM simulation, J. Geophys. Res., 113, C08041,

1090   doi:10.1029/2007JC004681, 2008.

1091

1092   Rau, H. G., Takahashi, T. and Des Marais, D. J.: Latitudinal variations in plankton

1093   δ13C: implications for CO2 and productivity in past oceans, Nature, 341, 516–518,

1094   1989.

1095

1096   Reimer, P. J., Bard, E., Bayliss, A., Beck, J. W., Blackwell, P. G., Ramsey, C. B., Buck,

1097   C. E., Cheng, H., Edwards, R. L., Friedrich, M., Grootes, P. M., Guilderson, T. P.,

1098   Haflidason, H., Hajdas, I., Hatté, C., Heaton, T. J., Hoffmann, D. L., Hogg, A. G.,

1099   Hughen, K. A., Kaiser, K. F., Kromer, B., Manning, S. W., Niu, M., Reimer, R. W.,

1100   Richards, D. A., Scott, E. M., Southon, J. R., Staff, R. A., Turney, C. S. M. and van der

1101   Plicht, J.: IntCal13 and Marine13 Radiocarbon Age Calibration Curves 0–50,000 Years

1102   cal BP, Radiocarbon, 55(4), 1869–1887, doi:10.2458/azu_js_rc.55.16947, 2013.

1103

1104   Rivera, P.: Beiträge zur Taxonomie und Verbreitung der Gattung Thalassiosira Cleve.

1105   Bibl. Phycol., 56, 1–220, 1981.

1106

1107   Round, E. E., Crawford, R. M. and Mann, D.G.: The Diatoms: biology and morphology

1108   of the genera. Cambridge University Press, Cambridge, 747 pp., 1990.

1109

1110   Rutllant, J. and Montecino, V.: Multiscale upwelling forcing cycles and biological

1111   response off north-central Chile, Rev. Chil. Hist. Nat., 75(1), 217–231,

1112   doi:10.4067/S0716-078X2002000100020, 2002.

1113

1114   Sabatier, P., Dezileau, L., Blanchemanche, P., Siani, G., Condomines, M., Bentaleb, I.

1115   and Piquès, G.: Holocene variations of radiocarbon reservoir ages in a mediterranean

1116   lagoonal system, Radiocarbon, 52(1), 91–102, doi:10.1017/S0033822200045057, 2010.

1117

1118   Saito, C., Noriki, S. and Tsunogai, S.: Particulate flux of Ai, a component of land

1119   origin, in the western North Pacific, Deep-Sea Res., 39, 1315–1327, 1992.

1120

1121   Salvatteci, R., Gutiérrez, D., Field, D., Sifeddine, A., Ortlieb, L., Bouloubassi, I.,

1122   Boussafir, M., Boucher, H. and Cetin, F.: The response of the Peruvian Upwelling

1123   Ecosystem to centennial-scale global change during the last two millennia, Clim. Past,

1124   10(2), 715–731, doi:10.5194/cp-10-715-2014, 2014.

1125

1126   Sarmiento, J. L. and Gruber, N.: Sinks for Anthropogenic Carbon, Phys. Today, 55(8),

1127   30–36, doi:10.1063/1.1510279, 2002.

1128

1129   Schneider, D. P. and Steig, E. J.: Ice cores record significant 1940s Antarctic warmth

1130   related to tropical climate variability, Proc. Natl. Acad. Sci., 105(34), 12154–12158,

1131   doi:10.1073/pnas.0803627105, 2008.

1132

1133   Schrader H. J. and Gersonde, R.: Diatoms and silicoflagellates. Utrecht Micropaleontol.

1134   Bull. 17, 129–176, 1978.

1135

1136 Shaffer, G., Pizarro, O. Djurfeldt, L., Salinas, S. and Rutllant, J.: Circulation and low-

1137 frequency variability near the Chilean coast: Remotely forced fluctuations during the

1138 1991– 92 El Niño, J. Phys. Oceanogr., 27, 217– 235, 1997.

1139

1140 Siebert, C., Nägler, T. F., von Blanckenburg, F., and Kramers, J. D.: Molybdenum

1141 isotope records as a potential new proxy for paleoceanography, Earth Planet. Sc. Lett.,

1142 211(1), 159–171, 2003.

1143

1144 Sun, X., Higgins, J. and Turchyn, A. V.: Diffusive cation fluxes in deep-sea sediments

1145 and insight into the global geochemical cycles of calcium, magnesium, sodium and

1146 potassium, Mar. Geol., 373, 64–77, doi:10.1016/j.margeo.2015.12.011, 2016.

1147

1148 Sundby, B., Martinez, P. and Gobeil, C.: Comparative geochemistry of cadmium,

1149 rhenium, uranium, and molybdenum in continental margin sediments, Geochim.

1150 Cosmochim. Ac., 68, 2485–2493, 2004.

1151

1152 Thomas, C. D., Bodsworth, E. J., Wilson, R. J., Simmons, A. D., Davies, Z. G.,

1153 Musche, M. and Conradt, L.: Ecological and evolutionary processes at expanding range

1154 margins, Nature, 411, 577−581, 2001.

1155

1156 Torres, M. E., Brumsack, H. J., Bohrman, G. and Emeis, K. C.: Barite front in

1157 continental margin sediments: a new look at barium remobilization in the zone of

1158 sulfate reduction and formation of heavy barites in diagenetic fronts, Chem. Geol., 127,

1159 125–139, 1996.

1160

1161 Torres, R., and Ampuero, P.: Strong CO2 outgassing from high nutrient low chlorophyll

1162 coastal waters off central Chile (30°S): The role of dissolved iron, Estuar. Coast. Shelf

1163 S., 83, 126−132, doi:10.1016/j.ecss.2009.02.030, 2009.

1164

1165 Tribovillard, N., Algeo, T. J., Lyons, T. and Riboulleau, A.: Trace metals as paleoredox

1166 and paleoproductivity proxies: an update. Chem. Geol., 232, 12–32, 2006.

1167

1168   Vance, D., Archer, C., Bermin, J., Perkins, J., Statham, P. J., Lohan, M. C., Ellwood, M.

1169   J. and Mills, R. A.: The copper isotope geochemistry of rivers and the oceans, Earth

1170   Planet. Sc. Lett., 274, 204–213, 2008.

1171

1172   Valle-Levinson, A., Moraga, J., Olivares, J. and Blanco, J. L.: Tidal and residual

1173   circulation in a semi-arid bay: Coquimbo Bay, Chile. Cont. Shelf Res., 20, 2009–2018,

1174   2000.

1175

1176   Valle-Levinson, A. and Moraga-Opazo, J.: Observations of bipolar residual circulation

1177   in two equatorward-facing semiarid bays, Cont. Shelf Res., 26(2), 179–193,

1178   doi:10.1016/j.csr.2005.10.002, 2006.

1179

1180   Van der Weijden, C.: Pitfalls of normalization of marine geochemical data

1181   using a common divisor, Mar. Geol., 184, 167–187, 2002.

1182

1183   Vargas, G., Ortlieb, L., Pichon, J. J., Bertaux, J. and Pujos, M.: Sedimentary facies and

1184   high resolution primary production inferences from laminated diatomacous sediments

1185   off northern Chile (23°S), Mar. Geol., 211(1–2), 79–99,

1186   doi:10.1016/j.margeo.2004.05.032, 2004.

1187

1188   Vargas, G., Pantoja, S., Rutllant, J., Lange, C. and Ortlieb, L.: Enhancement of coastal

1189   upwelling and interdecadal ENSO-like variability in the Peru-Chile Current since late

1190   19th century. Geophys. Res. Lett., 34, L13607, 2007.

1191

1192   Varma, V., Prange, M., Merkel, U., Kleinen, T., Lohmann, G., Pfeiffer, M., Renssen,

1193   H., Wagner, A. and Schulz, M.: Holocene evolution of the Southern Hemisphere

1194   westerly winds in transient simulations with global climate models. Clim. Past, 8, 391–

1195   402, doi:10.5194/cp-8-391-2012, 2012.

1196

1197   Wells, D. V., Hill, J. M., Park, M. J. and Williams, C. P.: The Shallow Sediments of the

1198   Middle Chincoteague Bay Area in Maryland: Physical and Chemical Characteristics.

1199   (Coastal and Estuarine Geology File Report No. 98-1): Maryland Geological Survey,

1200   Baltimore, MD., 104 pp., 1998.

1201

1202 Williams, P. M. and Gordon, L. I.: Carbon-13:carbon-12 ratios in dissolved and

1203 particulate organic matter in the sea. Deep-Sea Res., 17, 19−27, 1970.

1204

1205 Xu, G., Liu, J., Pei, S., Kong, X., Hu, G. and Gao, M.: Source identification of

1206 aluminum in surface sediments of the Yellow Sea off the Shandong Peninsula, Acta

1207 Oceanol. Sin., 34(12), 147–153, doi:10.1007/s13131-015-0766-9, 2015.

1208

1209 Zheng, Y., van Geen, A., Anderson, R. F., Gardner, J. V. and Dean, W. E.:

1210 Intensification of the northeast Pacific oxygen minimum zone during the Bölling-

1211 Alleröd warm period, Paleoceanography, 15, 528−536, 2000.

1212

1213 Zheng, Y., Anderson, R. F., van Geen, A. and Fleisheir, M.Q.: Preservation of non-

1214 lithogenic particulate uranium in marine sediments. Geochim. Cosmochim. Ac., 66,

1215 3085–3092, 2002.

1216

1226

Tables

Table 1. Concentration of elements in Pachingo wetland sediments, considered as lithogenic background for the study area. The values correspond to mean concentrations in surface sediments (0−3 cm).

Element	Metal/Al x 10^3	s
Ca	686.5	139.3
Fe	591.3	84.5
P	8.6	0.7
Sr	5.7	0.6
Ba	5.6	0.1
Cu	0.258	0.019
Ni	0.174	0.005
U	0.020	0.003
Mo	0.020	0.003
Cd	0.0021	0.0003
Re	0.00004	0.00001

Table 2. Radiocarbon dates for BGGC5 and BTGC8 sediment cores collected from mixed planktonic foraminifera and monospecific benthic foraminifera (*Bolivina plicata*), respectively. The ^{14}C-AMS was performed at NOSAM-WHOI. The lab code and conventional ages collected from each core section is indicated. For error calculations see http://www.whoi.edu/nosams/radiocarbon-data-calculations.

Core identification	material	mass (mg)	Lab. Code NOSAM	modern fraction pMC	error	Conventional BP	Age error
BGGC5							
10-11	Planktonic foraminifera (mix)	1.8	OS-122160	0.8895	0.0027	940	25
18-19	Planktonic foraminifera (mix)	1.1	OS-122141	0.7217	0.0024	2,620	25
31-32	Planktonic foraminifera (mix)	2.7	OS-122161	0.6590	0.0021	3,350	25
45-46	Planktonic foraminifera (mix)	2	OS-122162	0.6102	0.0017	3,970	25
55-56	Planktonic foraminifera (mix)	1.6	OS-122138	0.5864	0.0025	4,290	35
66-67	Planktonic foraminifera (mix)	2.8	OS-122304	0.5597	0.0018	4,660	25
76-77	Planktonic foraminifera (mix)	2.6	OS-122163	0.4520	0.0016	6,380	30
96-97	Planktonic foraminifera (mix)	1.1	OS-122139	0.4333	0.0033	6,720	60
115-116	Planktonic foraminifera (mix)	4.7	OS-122164	0.3843	0.0016	7,680	35
125-126	Planktonic foraminifera (mix)	1.4	OS-122140	0.3964	0.0025	7,430	50
BTGC8							
5-6	Benthic foraminifera (*Bolivina plicata*)	4.2	OS-130657	0.8953	0.0017	890	15
20-21	Benthic foraminifera (*Bolivina plicata*)	7.7	OS-123670	0.7337	0.0021	2,490	25
30-31	Benthic foraminifera (*Bolivina plicata*)	13	OS-123671	0.6771	0.0016	3,130	20
40-41	Benthic foraminifera (*Bolivina plicata*)	11	OS-123672	0.6507	0.0019	3,450	25
50-51	Benthic foraminifera (*Bolivina plicata*)	8.7	OS-123673	0.5877	0.0014	4,270	20
60-61	Benthic foraminifera (*Bolivina plicata*)	13	OS-123674	0.5560	0.0018	4,720	25
71-72	Benthic foraminifera (*Bolivina plicata*)	10	OS-123675	0.4930	0.0013	5,680	20
80-81	Benthic foraminifera (*Bolivina plicata*)	7.3	OS-123676	0.4542	0.0012	6,340	20
90-91	Benthic foraminifera (*Bolivina plicata*)	6.8	OS-123677	0.4259	0.0015	6,860	30
96-97	Benthic foraminifera (*Bolivina plicata*)	6.8	OS-123678	0.3903	0.0013	7,560	25

Table 3. Reservoir age (DR) estimation considering the ^{210}Pb age determined with the CRS model (McCaffrey and Thomson, 1980) at a selected depth sections of the core, compared with ^{14}C ages (yr BP) from marine13.14 curve (Reimer et al., 2013), according to Sabatier et al. (2010).

Core	cm	Age from CRS model	Age years BP[a]	[14]C marine13 curve	[14]C age BP from foram.	DR	s
BGGC5	10.5	1828	122	499	940	441	15
BTCG8	5.5	1908	42	448	890	442	17

a. Before present=1950

Table 4. Spearman rank order correlations for geochemical data. Significant values >0.8 are indicated in bold.

BGGC5

	Al	P	K	Ca	Mn	Fe	Ni	Cu	Mo	Cd	Re	Sr	U	Ba	Opal	TOC
Al	1.00	-0.62	0.49	-0.48	0.64	0.60	-0.75	0.56	-0.10	-0.73	-0.08	-0.33	0.08	0.49	-0.52	-0.44
P		1.00	-0.31	0.37	-0.45	-0.56	0.56	-0.57	0.01	0.61	-0.11	0.39	-0.12	-0.20	0.49	0.24
K			1.00	-0.24	**0.90**	**0.83**	-0.29	0.47	0.28	-0.42	0.33	-0.12	0.50	0.26	-0.25	-0.19
Ca				1.00	-0.47	-0.50	0.44	-0.64	0.23	0.59	0.39	**0.92**	0.30	-0.60	0.18	0.32
Mn					1.00	**0.94**	-0.51	0.68	-0.01	-0.68	0.07	-0.32	0.24	0.43	-0.39	-0.31
Fe						1.00	-0.49	**0.81**	0.03	-0.70	0.11	-0.40	0.23	0.36	-0.37	-0.21
Ni							1.00	-0.51	0.49	**0.91**	0.35	0.25	0.26	-0.70	0.72	0.64
Cu								1.00	-0.12	-0.71	-0.06	-0.61	0.00	0.31	-0.39	-0.07
Mo									1.00	0.50	**0.88**	0.10	0.91	-0.48	0.33	0.36
Cd										1.00	0.36	0.42	0.27	-0.67	0.70	0.54
Re											1.00	0.27	**0.92**	-0.50	0.16	0.38
Sr												1.00	0.24	-0.36	0.05	0.17
U													1.00	-0.39	0.10	0.29
Ba														1.00	-0.30	-0.59
Opal															1.00	0.35
TOC																1.00

BTGC8

	Al	P	K	Ca	Mn	Fe	Ni	Cu	Mo	Cd	Re	Sr	U	Ba	Opal	TOC
Al	1.00	-0.19	-0.17	-0.37	-0.02	-0.03	-0.39	-0.04	-0.39	0.02	-0.13	-0.58	-0.19	0.07	-0.41	-0.29
P		1.00	0.23	0.00	0.43	0.28	0.58	0.23	0.37	0.13	-0.04	0.30	0.14	-0.14	0.56	0.13
K			1.00	-0.02	0.54	0.41	0.43	0.22	-0.11	0.05	-0.04	0.19	-0.28	0.28	0.26	0.20
Ca				1.00	-0.33	-0.27	0.00	-0.23	0.39	0.01	0.33	0.50	0.47	-0.34	0.20	0.34
Mn					1.00	0.21	0.64	0.01	0.05	0.33	0.15	0.32	-0.02	0.24	0.32	0.00
Fe						1.00	0.13	0.71	-0.40	-0.48	-0.67	-0.37	-0.62	0.13	0.14	0.10
Ni							1.00	0.24	0.56	0.20	0.25	0.64	0.19	-0.16	**0.80**	0.45
Cu								1.00	-0.25	-0.68	-0.56	-0.22	-0.61	-0.10	0.21	0.37
Mo									1.00	0.45	0.59	0.66	0.69	-0.41	0.58	0.30
Cd										1.00	0.56	0.39	0.52	0.11	0.10	-0.12
Re											1.00	0.53	**0.83**	-0.16	0.13	0.17
Sr												1.00	0.58	-0.13	0.52	0.23
U													1.00	-0.19	0.21	0.00
Ba														1.00	-0.28	-0.42
Opal															1.00	0.39
TOC																1.00

Figures
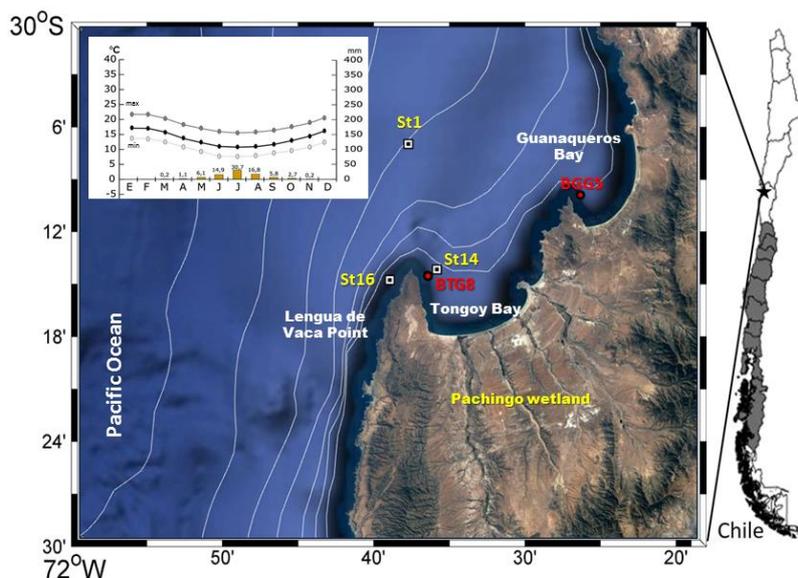
Figure 1. Study area showing the position of sampling stations. Sediment cores were retrieved from Guanaqueros Bay (BGGC5) and from Tongoy Bay (BTGC8) at water depths of 89 and 85 m, respectively. Information of dissolved oxygen (DO) in the water column and of suspended organic particles collected at ST1, ST14 and ST16 sampling sites was gathered in a previous project (INNOVA 07CN13 IXM-150). Climograph of the region is showing the average precipitation in mm (bars) and temperatures in °C (min, max and average) over 12-month period.
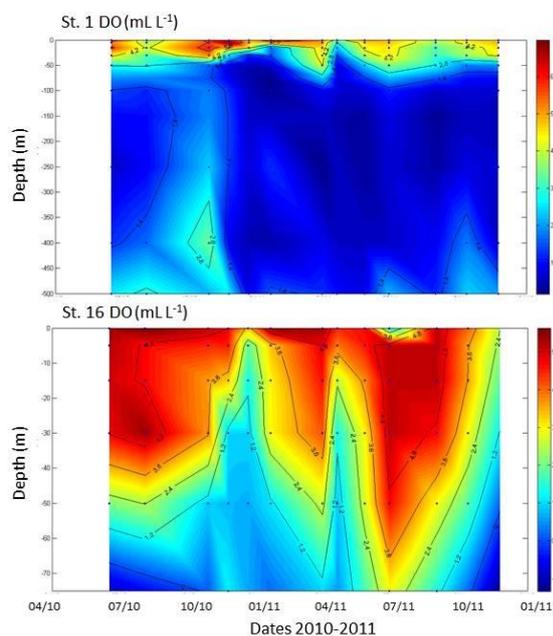
Figure 2. Dissolved Oxygen (DO) time series in the water column measured between October 2010 and January 2011, at stations St1 and St16 off Tongoy Bay, Coquimbo (30°S).
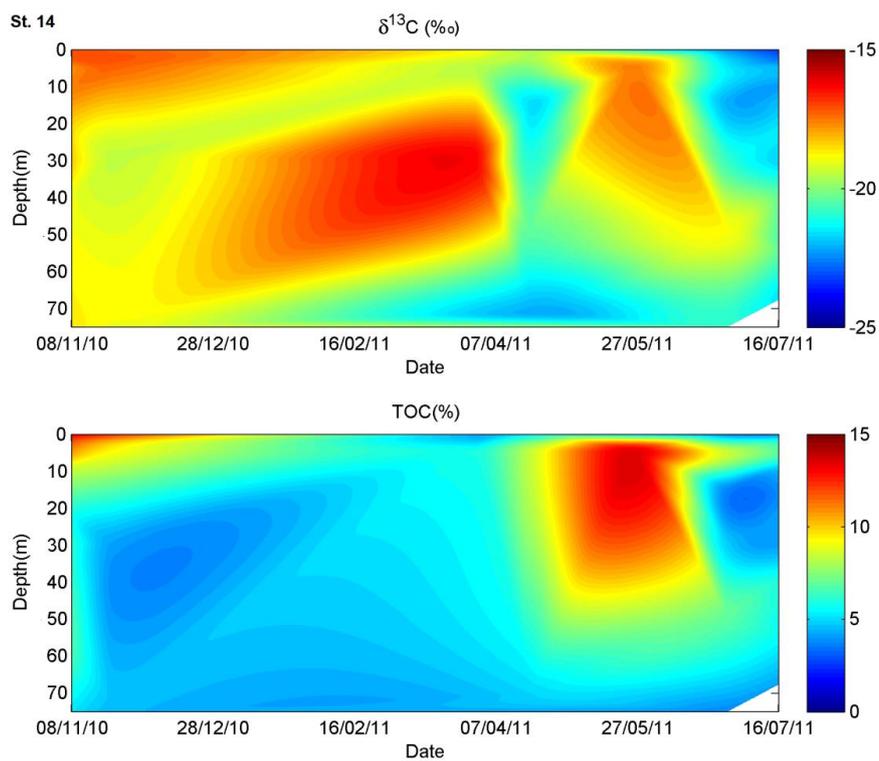
Figure 3. Suspended particulate matter composition (TOC % and δ^{13}Corg) measured in the water column between October 2010 and October 2011, at station St14, Tongoy Bay, Coquimbo (30°S).
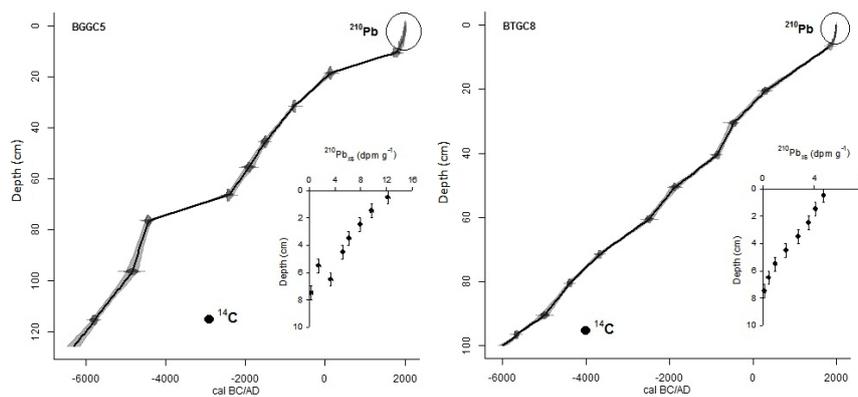
Figure 4. Age model based on [14]CAMS and ^{210}Pb measurements. The time scale was obtained according to the best fit of curves of $^{210}Pb_{xs}$ and ^{14}C points using CLAM 2.2 software and Marine curve [13]C (Reimer et al., 2013).

a)
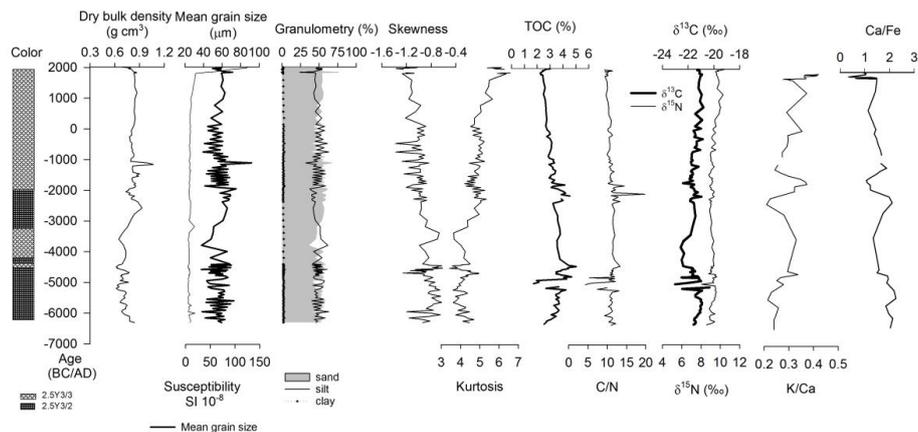
b)
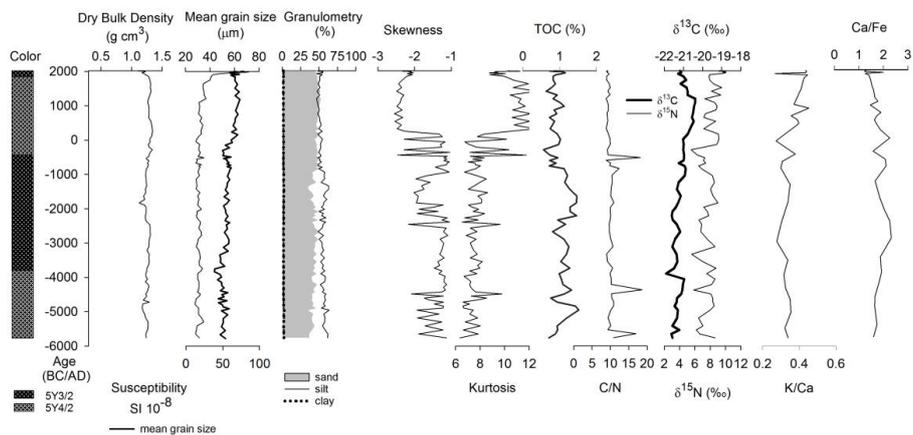
Figure 5. Sediment characterization of sediment cores retrieved from (a) Guanaqueros Bay (BGGC5) and (b) Tongoy Bay (BTGC8). Distribution in depth core of color, dry bulk density, statistical parameters (skewness, mean grain size, kurtosis), organic components (TOC, stable isotopes) and chemical composition (K/Ca, Ca/Fe).

a)
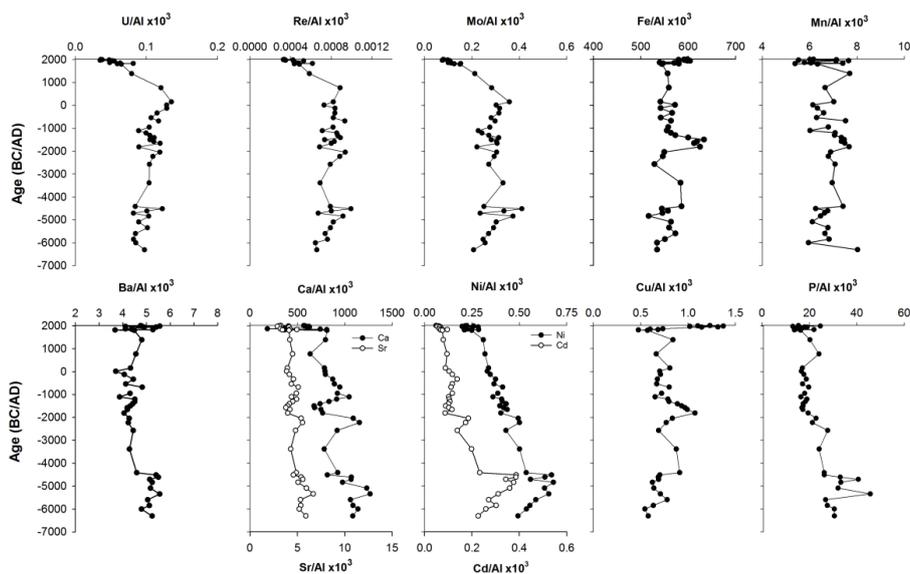
b)
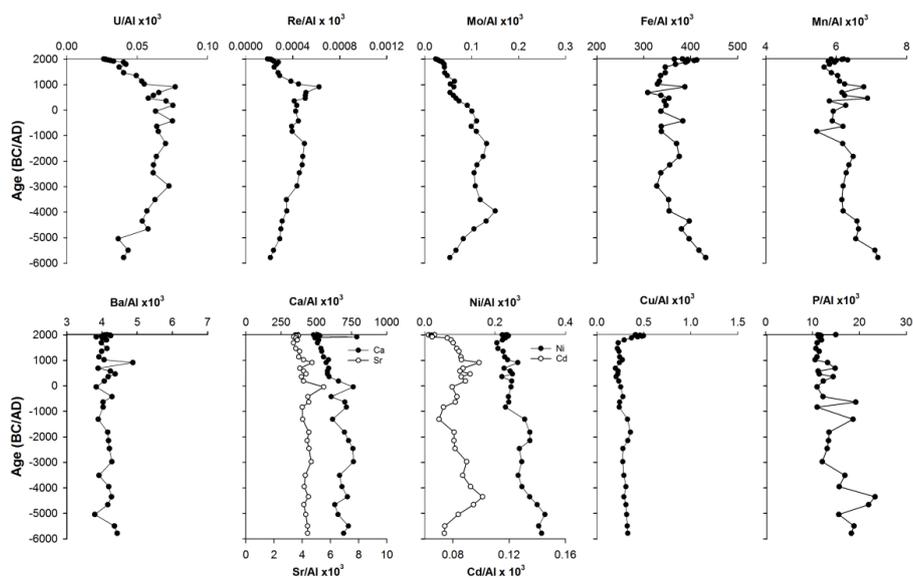
Figure 6. Trace element distribution in sediment cores retrieved from (a) Guanaqueros
Bay (BGGC5) and (b) Tongoy Bay (BTGC8), off Coquimbo (30°S).
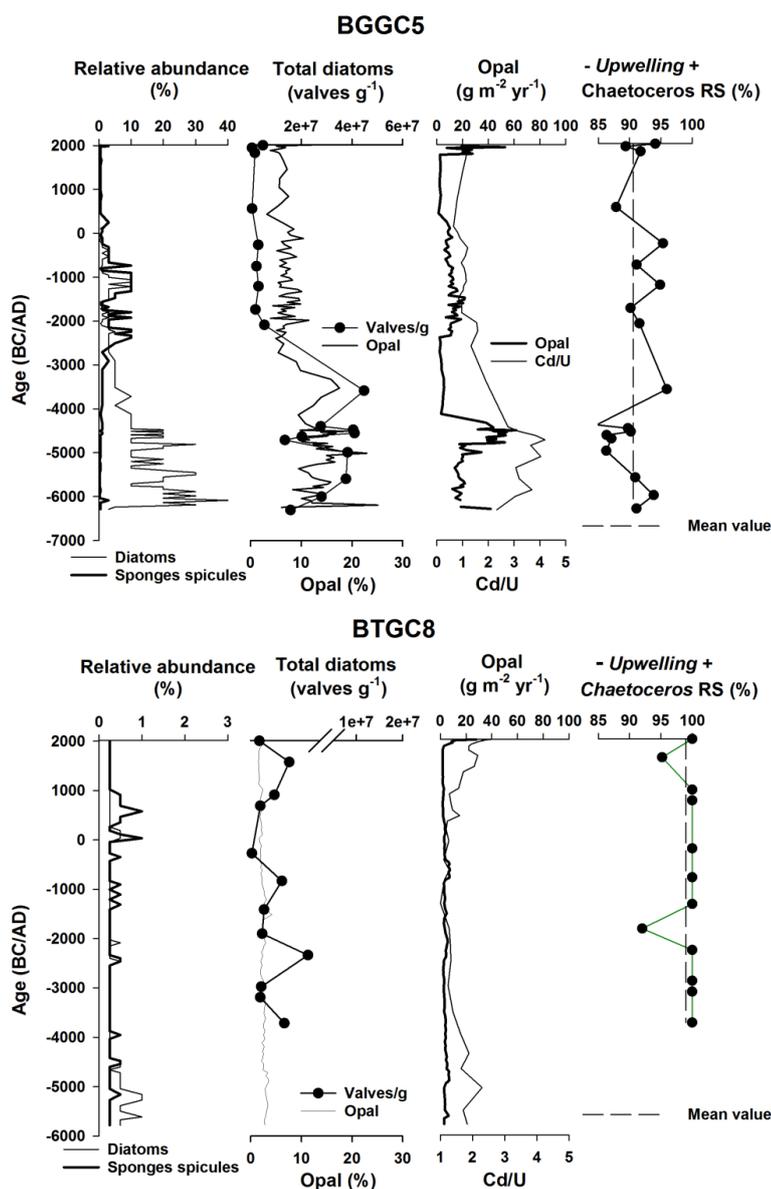
Figure 7. Diatom abundance, opal accumulation and temporal variations in the relative abundance of *Chaetoceros* resting spores in BGGC5 and BTGC8 cores (Guanaqueros and Tongoy Bay, respectively). Cd/U distribution was included as a proxy for redox condition.
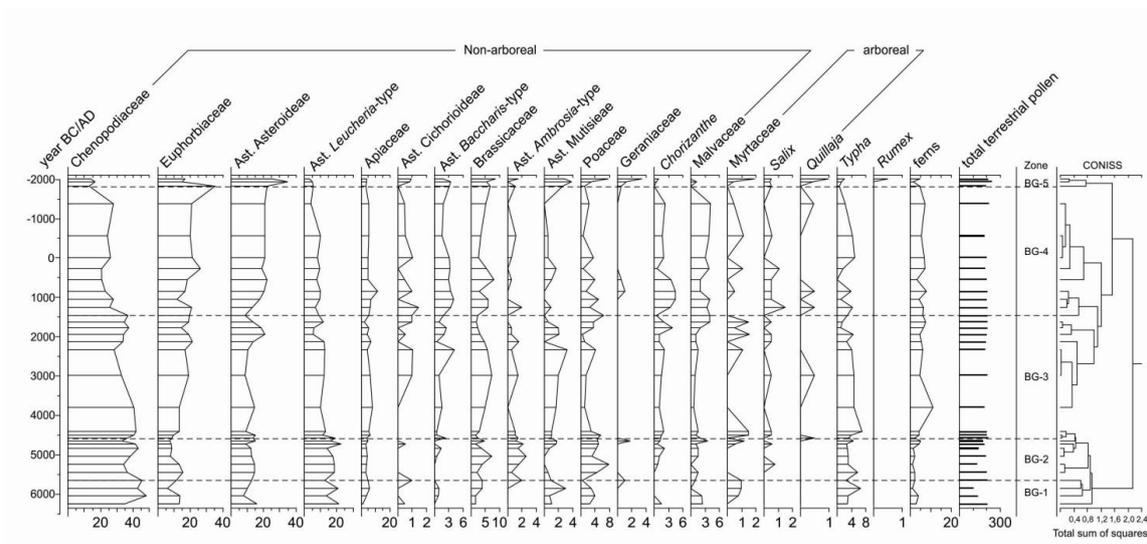
Figure 8. Pollen record in BGGC5 core.
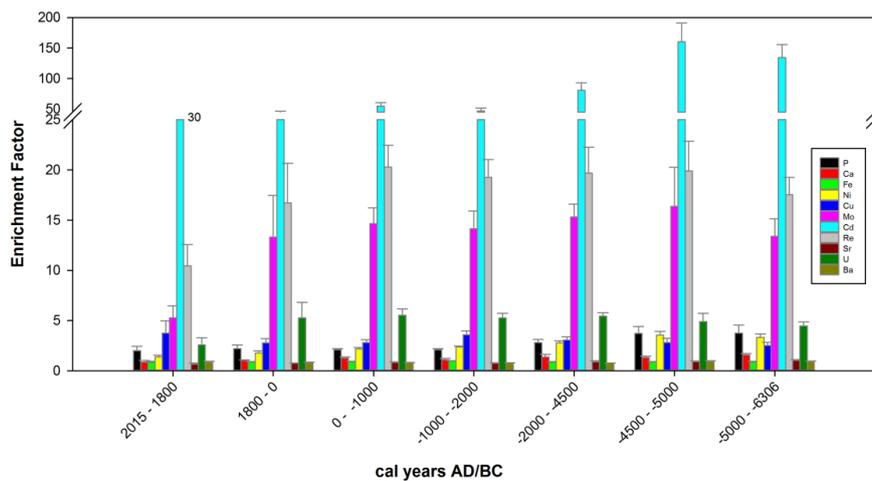
Figure 9. Authigenic enrichment factor (EF) of trace elements in BGGC5 core. Lithogenic background as estimated from surface sediments of Pachingo wetland cores (see text).
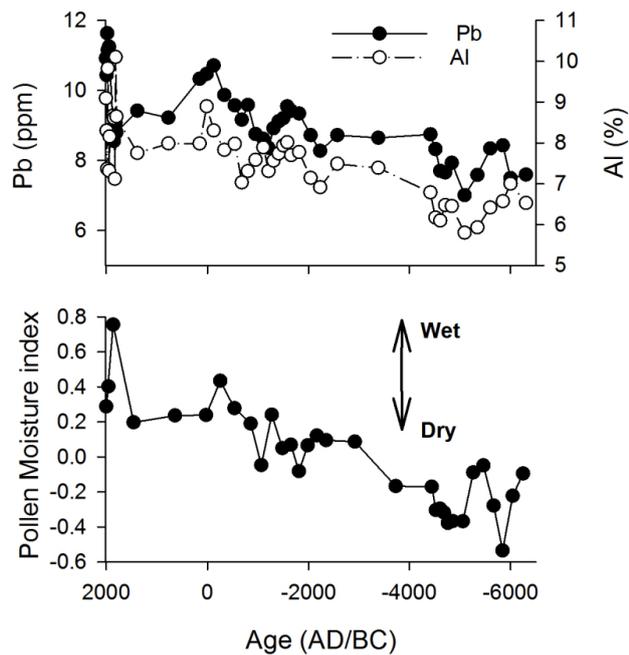
Figure 10. Pollen Moisture Index defined as the normalized ratio between Euphorbiaceae (wet coastal shrub land) and Chenopodiaceae (arid scrubland). Positive (negative) values for this index indicate the relative expansion (reduction) of coastal vegetation under wetter (drier) conditions. Pb and Al distribution at BGGC5 core, representatives of terrigenous input to the bay.